ESA Climate Change Initiative (CCI+)

Climate Assessment Report (CAR)

for Climate Research Data Package No. 8 (CRDP#8)

of the Essential Climate Variable (ECV)

Greenhouse Gases (GHG)

Project: GHG-CCI+

Frédéric Chevallier [a] and Julia Marshall[b]

[a] Laboratoire des Sciences du Climat et de l'Environnement (LSCE), Gif-sur-Yvette, France

[b] Institut für Physik der Atmosphäre, Deutsches Zentrum für Luft- und Raumfahrt (DLR), Oberpfaffenhofen, Germany

Change log:

Version Nr.	Date	Status	Reason for change
Version 0.0	Sept. 2023	Initial draft	User assessment for CRDP#8 XCO_2 products
Version 1.0	8 Feb. 2024	Approved	User assessment for CRDP#8 with XCH_4 products, update of the literature review for CH_4 and (to a lesser degree) CO_2 inversions.

This document should be cited as:

Chevallier, F. and Marshall, J., Climate Assessment Report for Climate Research Data Package No. 8 (CRDP#8) of ESA's Climate Change Initiative project GHG-CCI+, version 1.0, 8 Feb. 2024, 2024.

Table of contents

	ESA Climate Change Initiative (CCI+)	Page 4
ghg cci	**Climate Assessment Report (CAR)** for Climate Research Data Package 8 (CRDP#8)	Version 1.0
	of the Essential Climate Variable (ECV) Greenhouse Gases (GHG)	8 February 2024

1. Executive summary

This report describes the **assessment of the Essential Climate Variable (ECV) data products of the eigth release of the GHG-CCI Climate Research Data Package** (CRDP#8) by the Climate Research Group (CRG) of the GHG-CCI+ project (Buchwitz et al. 2015, 2017; see also GHG-CCI+ website https://climate.esa.int/en/projects/ghgs/). These products are CO_2 and CH_4 column retrievals (XCO$_2$ and XCH$_4$) from current satellite instruments:

- **CO2_OC2_FOCA:** XCO$_2$ from NASA's OCO-2 satellite retrieved by University of Bremen using the FOCAL algorithm (global, Sep. 2014 – February 2022, v10.1)
- XCO$_2$ and XCH$_4$ from Japan's GOSAT-2 satellite (products **CO2_GO2_SRFP**, **CH4_GO2_SRFP**, **CH4_GO2_SRPR**, global, Feb. 2019 – December 2021, v2.0.2)
- **CH4_S5P_WFMD:** XCH$_4$ from the European Sentinel-5-Precursor (S5P) satellite retrieved by University of Bremen using the WFM-DOAS algorithm (global, Nov. 2017 – Dec. 2022, v1.8)

These products will be available via the CCI Open Data Portal (https://climate.esa.int/en/odp/#/dashboard).

Climate researchers may find interest in these products for various reasons like evaluating climate models, estimating the uncertain parameters of these climate models, studying the variability of CO_2 and CH_4 in the atmosphere, studying wildfire or fossil fuel emission plumes, or quantifying the surface fluxes of these gases.

CRDP#8 is the fourth release of products from the GHG-CCI+ project, which started in March 2019.

Datasets CRDP#1 to CRDP#4 have been generated and released by the GHG-CCI pre-cursor project (2010 - 2018). These products are CO_2 and CH_4 products from SCIAMACHY/ENVISAT, MIPAS/ENVISAT, GOSAT, AIRS and IASI. The XCO$_2$ and XCH$_4$ and IASI products are now generated operationally via the Copernicus Climate Change Service (C3S, https://climate.copernicus.eu/) and are available via the Copernicus Climate Data Store (CDS, https://cds.climate.copernicus.eu/).

By producing retrievals of the CO_2 and CH_4 columns for these satellites and others, CRDP has given a **unique**, though heterogeneous, **climate record from space covering now more than twenty years** of the two major greenhouse gases of anthropogenic origin. **This length opens the possibility to characterize emission trends, as was already demonstrated by a series of CRDP-based studies for CH$_4$** (e.g., Bergamaschi et al. 2013, Schneising et al., 2020) **and for CO$_2$** (e.g., Ross et al. 2013, Schneising et al. 2013a, 2013b, Reuter et al. 2014b, Detmers et al. 2015). For the entire publication list please see https://climate.esa.int/en/projects/ghgs/publications/.

Previous iterations of the CRDP explored an ensemble-based approach to make use of the range of retrieval product covering several sensors and multiple retrieval algorithms (EMMA). **This ensemble approach allowed for a more comprehensive assessment of the product uncertainty than just the**

	ESA Climate Change Initiative (CCI+)	Page 5
ghg cci	**Climate Assessment Report (CAR)** for Climate Research Data Package 8 (CRDP#8)	Version 1.0
	of the Essential Climate Variable (ECV) Greenhouse Gases (GHG)	8 February 2024

typical uncertainty characterisation of each product through internal uncertainty propagation. Reuter et al. (2013, 2014a, 2020) illustrated this capability well.

The CRDP data sets, together with satellite retrievals made outside Europe, have served to **quantify regional carbon budgets** (e.g., Basu et al. 2013, Bergamaschi et al. 2013, Fraser et al. 2013, Monteil et al. 2013, Cressot et al. 2013, to cite only early ones) and more specifically (for CO_2) Canada and Siberian forests (Schneising et al. 2011), Eurasia (Guerlet et al. 2013a), Tropical Asia (Basu et al. 2014), Amazonia (Parazoo et al. 2013) and Europe (Reuter et al. 2014a). However, for CO_2, there remains considerable discrepancies among inversions driven by satellite retrievals, and also between these ones and bottom up estimates or inversions based on atmospheric in-situ observations (Chevallier et al. 2014a, 2019, Feng et al. 2016a, Reuter et al. 2016c). These discrepancies were also highlighted in the first seven releases of the CAR (Chevallier et al. 2013, 2015, 2016, 2017; Chevallier 2020; Chevallier and Marshall 2021, 2023). For CH_4 it has been early and clearly demonstrated that the SCIAMACHY retrievals and the GOSAT retrievals provide important information on regional methane emissions (e.g., Bergamaschi et al. 2013, Fraser et al. 2013, Alexe et al. 2015).

Each application of the CRDP has specific user requirements (e.g., Chevallier et al., 2014b) and it is not possible to exhaustively cover them in the CRG. Instead, the CRG has focussed on global source-sink inversion from several viewpoints.

For CO_2, this study has covered the two XCO_2 products of CRDP#8: CO2_OC2_FOCA which has been retrieved from OCO-2, and CO2_GO2_SRFP which has been retrieved from GOSAT-2. The assimilation of the CRDP#8 products in the CAMS/LSCE global inversion system infers a latitudinal distribution of CO_2 surface fluxes that is very different from that obtained by the assimilation of surface air-sample measurements or the assimilation of NASA's retrievals from OCO-2. We think that it is less credible because it yields a poorer simulation of the atmospheric growth rate and a poorer fit to independent atmospheric measurements.

The consistent results obtained in the CAMS inversions between the surface air-sample measurements and the ACOS retrievals demonstrates that there is no fundamental limitation in atmospheric inverse modelling (e.g., in the realism of the transport model or in the modelled error statistics) when assimilating satellite XCO_2 retrievals. The ACOS-driven CO_2 surface fluxes have actually been part of the official CAMS data portfolio since year 2019 and several ACOS-driven inversions pass the quality control of Global Carbon Project's Global Carbon Budget (Friedlingstein et al. 2022).

ACOS and CO2_OC2_FOCA exploit the same OCO-2 spectra. The various tests performed do not allow us to identify the distinctive asset of ACOS in our system: the data precision (that seem to be better for ACOS according to the reported uncertainty of each product), the data trueness (linked to the quality of the physical retrieval scheme and to its empirical bias-correction), the accuracy of the averaging kernels (see Chevallier, 2015, for a discussion on potential issues with the averaging kernel profiles), or a combination of these qualities at once. These hypotheses implictely involve the retrieval quality control. Detailed sensitivity tests could be performed for this, but note that our

single CO2_OC2_FOCA-driven inversion already represented a large computational effort that lasted ten days on a supercomputer.

For CO2_GO2_SRFP, we note that so far GOSAT-driven inversions have not reach the quality of OCO-2 driven ones to our best knowledge, and we may meet such a limitation with GOSAT-2 as well, due to the instrument quality joined to its sampling strategy. However, even with this challenge in mind, the simulation of the atmospheric growth rate still seems to be particularly poor.

About computational effort, CO2_OC2_FOCA's distinct advantage compared to ACOS is its representation of multiple scattering effects in the radiative transfer in a form that is not costlier than absorption. In preparation for the Copernicus CO_2 Monitoring Mission that will provide even larger amount of data than OCO-2 (Pinty et al., 2017), the processing of the OCO-2 archive, which is very large by today's standards, by CO2_OC2_FOCA represents an important achievement. In this context and resources permitting, it would be important to document their performance in more detail in order to help prioritize future developments.

For CH$_4$, the WFMD retrieval product, CH4_S5P_WFMD, based on TROPOMI measurements from S5P, is not the only data product that covers multiple years. In order to expand the scope of this assessment, the operational S5P retrieval using the RemoTeC algorithm (v2.5.0, hereafter referred to as CH4_S5P_SRON) has been included in the assessment. Previous versions of the CAR also included the "scientific" retrieval from SRON, which included improvements to their retrieval that had not yet been integrated into the operational product. With the latest version of the operational algorithm, however, these differences are now very minor, and only the operational version of the retrieval algorithm was included in this round of the assessment. Another difference from CAR7 is the longer data period available from the GOSAT retrievals, allowing for an assessment including inversions for the first time.

The comparison begins by comparing the XCH$_4$ products to an inversion optimized using surface-based measurements from around the world. Thanks to the ever-improving timeliness of the data set available through the cooperative ObsPack initiative, it was possible to include 91 sites in the surface-based inversion. This is based on the standard ObsPack release 5.1 (obspack_ch4_1_GLOBALVIEWplus_v5.1_2023-03-08, Schuldt et al., 2023), augmented with the near-real-time product for measurements in 2022 (obspack_ch4_1_NRT_v5.1_2023-02-21, Schuldt et al., 2023). In general, satellite retrievals are available for use with much less lag time than are contemporaneous in-situ measurements, which is a limitation when assessing retrievals less than a year after the measurement time.

The comparison of the surface-optimized concentration fields with the satellite products shows a systematic offset with a latitudinal dependence, attributable to errors in the transport model due to poorly represented tropopause height and stratospheric gradients. In order to not map this transport error onto the resultant fluxes, a 2nd order polynomial correction is applied. Assessing the shape of this correction shows that the latitudinal gradients of the CH4_S5P_WFMD retrievals from the commissioning phase (prior to April 2018) are somewhat different than the same months in following

years. After this, the shape of the bias correction is roughly stable for each month, allowing for a bias correction to be projected onto more recent satellite measurements, when surface measurements are not available as a constraint. No land-sea bias is seen in the derived bias corrections for CH4_S5P_WFMD and CH4_S5P_SRON (though the latter has few data over the oceans), and the two different GOSAT-2 retrievals (SRFP and SRPR) also result in similar curves.

Inversions were carried out using CH4_S5P_WFMD and CH4_S5P_SRON from January 2018 through December 2022. As no retrievals are available for the operational product and fewer from the WFMD retrieval during the commissioning period, results for early 2018 should not be overinterpreted. For CH4_GO2_SRFP and CH4_GO2_SRPR, inversions were carried out for two years, from January 2019 through December 2021. This is despite the fact that the data product only contains measurements from February 2019: due to a technical limitation of the inversion system, inversions must always begin in January of a given calendar year, although they can end at any point during a year.

The assimilation of the S5P retrievals in the Jena CarboScope global inversion system results in methane fluxes that are largely similar in spatial distribution from those obtained by the assimilation of surface air-sample measurements, which is a change from the last CAR. This may be related to the better data coverage of the surface-based network, with almost three times as many stations being included. In general, the flux increments seen for the overlapping years for the GOSAT-2 and S5P retrievals agree with each other, in particular with respect to increasing fluxes over the eastern Amazon (consistent with the findings of Basso et al., 2021), eastern Africa (as in Lunt et al., 2019), and Indonesia, while decreasing emissions in boreal regions, much of China, and in higher latitudes in the Southern Hemisphere. The resultant global mean near-surface concentrations show comparable variability to and good correlation with global mean concentration estimates from NOAA and WDCGG, based on in-situ measurements. The time period is quite short, making it difficult to make robust conclusions about the derived global growth rates, but also here the results between the different inversions are statistically consistent with one another.

In the assessment of the global mean near-surface concentration, the CH4_GO2_SRPR and CH4_GO2_SRFP inversions correlated slightly better with the NOAA and WDCGG estimates, suggesting a better consistency with the surface measurements on a global scale. Between the CH4_GO2_SRPR and CH4_GO2_SRFP inversions, the CH4_GO2_SRFP fluxes showed more spatial coherence.

The concentration fields resulting from the optimized fluxes were compared to independent measurements, namely aircraft profiles and total column measurements from the TCCON network of surface-based Fourier Transform Spectrometers. These results show that that satellite-based inversions agree better with TCCON than does the surface-based inversion, while the aircraft-based measurements tend to agree better with the concentrations constrained from the surface network.

2. User related aspects discussed in the peer-reviewed literature

The GHG-CCI project primarily aims at bringing new knowledge about the sources and sinks of CO_2 and CH_4 based on satellite-derived data products. Since the start of Phase 1 of the GHG-CCI pre-cursor project in 2010, this aspect has been addressed in a series of publications, which are shortly summarised in the following. They usefully provide the background for the new studies that have been performed specifically for this report and that will be described next. For a full list of publications see "Project publications" on https://climate.esa.int/en/projects/ghgs/publications/.

We start with the publications related to natural CO_2 fluxes.

- Using global GOSAT XCO_2 retrievals, Basu et al. (2013) presented first global CO_2 surface flux inverse modelling results for various regions. Their analysis suggested a reduced global land sink and a shift of the carbon uptake from the tropics to the extra-tropics. In particular, their results suggested that Europe is a stronger carbon sink than expected, but this feature was not further discussed in this paper.
- Chevallier et al. (2014a) analysed an ensemble of global inversion results assimilating two GOSAT XCO_2 retrieval products. They found hemispheric and regional differences in posterior flux estimates that are beyond 1 sigma uncertainties. They too found a significantly larger European carbon sink or a larger North African emission than expected. They concluded to the existence of significant flaws in all main components of the inversions: the transport model, the prior error statistics and the retrievals.
- Houweling et al. (2015) presented the outcome of a large inverse modelling intercomparison experiment on the use of GOSAT retrievals. The ensemble of results confirmed the large latitudinal shift in carbon uptake, but they showed that the reduced gradient degrades the agreement with background aircraft and surface measurements.
- Reuter et al. (2014a) investigated the European carbon sink further with another ensemble of GOSAT XCO_2 products, a SCIAMACHY XCO_2 product and a new inversion method which is less sensitive to some of the issues discussed in Chevallier et al. (2014a). Reuter et al. (2014a) only used satellite XCO_2 retrievals over Europe to rule out that non-European satellite data adversely influence the European results and they also only used short-term (days) transport modelling to avoid long-range transport errors. Based on an extensive analysis they concluded: "We show that the satellite-derived European terrestrial carbon sink is indeed much larger (1.02 ± 0.30 GtC/year in 2010) than previously expected". The value they derived is significantly larger compared to bottom-up estimates (not based on atmospheric measurements) of 0.235 ± 0.05 GtC/year for 2001-2004 (Schulze et al, 2009).
- The findings of Reuter et al. (2014a) stimulated additional research (Feng et al. 2016a, Reuter et al. 2016c).
- Detmers et al. (2015) analyzed GOSAT XCO_2 retrievals to detect and quantify anomalously large carbon uptake in Australia during a strong La Niña episode.
- For flux inversions, not only the retrieved greenhouse gas values are relevant, but also their error statistics, in particular the reported uncertainties. Chevallier and O'Dell (2013) analyzed this aspect in the context of CO_2 flux inversions using GOSAT XCO_2 retrievals. For CH_4, Cressot et al. (2013, 2016) studied the uncertainty of flux inversions assimilating SCIAMACHY, GOSAT or IASI XCH_4 retrievals.
- Focussing on Canadian and Siberian boreal forests, Schneising et al. (2011) computed longitudinal XCO_2 gradients from SCIAMACHY XCO_2 retrievals during the vegetation growing season over Canadian and Siberian boreal forests and compared the gradients with outputs from NOAA's CO_2 assimilation system CarbonTracker (Peters et al. 2007). They found good agreement for the total

	ESA Climate Change Initiative (CCI+)	Page 9
ghg cci	**Climate Assessment Report (CAR)** for Climate Research Data Package 8 (CRDP#8)	Version 1.0
	of the Essential Climate Variable (ECV) Greenhouse Gases (GHG)	8 February 2024

boreal region and for inter-annual variations. For the individual regions, however, they found systematic differences suggesting a stronger Canadian boreal forest growing season CO_2 uptake and a weaker Siberian forest uptake compared to CarbonTracker.

- Focussing on hemispheric data and on carbon-climate feedbacks, Schneising et al. (2014a) used SCIAMACHY XCO_2 to study aspects related to the terrestrial carbon sink by looking at co-variations of XCO_2 growth rates and seasonal cycle amplitudes with near-surface temperature. They found XCO_2 growth rate changes of 1.25 ± 0.32 ppm/year/K (approximately 2.7 ± 0.7 GtC/year/K; indicating less carbon uptake in warmer years, i.e., a positive carbon-climate feedback) for the Northern Hemisphere in good agreement with CarbonTracker.

- Reuter et al. (2013) computed CO_2 seasonal cycle amplitudes using various satellite XCO_2 data products (using GHG-CCI products but also GOSAT XCO_2 products generated in Japan at NIES (Yoshida et al. 2013, Oshchepkov et al. 2013) and the NASA ACOS product (O'Dell et al. 2012) and compared the amplitudes with TCCON and CarbonTracker. They found that the satellite products typically agree well with TCCON but they found significantly lower amplitudes for CarbonTracker suggesting that CarbonTracker underestimates the CO_2 seasonal cycle amplitude by approx. 1.5 ± 0.5 ppm (see also Buchwitz et al., 2015, for a discussion of these findings).

- Lindquist et al. (2015) compared satellite XCO_2 retrievals, surface XCO_2 retrievals and atmospheric model simulations in terms of XCO_2 seasonal cycle. They found that the satellite retrieval algorithms performed qualitatively similarly but showed notable scatter at most validation sites. None of the tested algorithm clearly outperformed another. They showed that the XCO_2 seasonal cycle depends on longitude especially at the mid-latitudes, which was only partially shown by the models. They also found that model-to-model differences could be larger than GOSAT-to-model differences.

- Guerlet et al. (2013a) analyzed GOSAT XCO_2 retrievals focusing on the Northern Hemisphere. They identified a reduced carbon uptake in the summer of 2010 and found that this is most likely due to the heat wave in Eurasia driving biospheric fluxes and fire emissions. Using a joint inversion of GOSAT and surface data, they estimated an integrated biospheric and fire emission anomaly in April–September of 0.89 ± 0.20 PgC over Eurasia. They found that inversions of surface measurements alone fail to replicate the observed XCO_2 inter-annual variability (IAV) and underestimate emission IAV over Eurasia. They highlighted the value of GOSAT XCO_2 in constraining the response of land-atmosphere exchange of CO_2 to climate events.

- Basu et al. (2014) studied seasonal variation of CO_2 fluxes during 2009-2011 over Tropical Asia using GOSAT, CONTRAIL and IASI data. They found an enhanced source for 2010 and concluded that this is likely due to biosphere response to above-average temperatures in 2010 and unlikely due to biomass burning emissions.

- Parazoo et al. (2013) used GOSAT XCO_2 and solar induced chlorophyll fluorescence (SIF) retrievals to better understand the carbon balance of southern Amazonia.

- Ross et al. (2013) used GOSAT data to obtain information on wildfire CH_4:CO_2 emission ratios.

- The strong El Niño event of 2015-2016, shortly after the launch of OCO-2, provided an opportunity to assess the carbon-climate feedbacks using satellite data, e.g. Liu et al. (2017) and Chatterjee et al. (2017).

Despite the fact that none of the existing satellite missions has been optimized to obtain information on anthropogenic CO_2 emissions, this important aspect has been addressed in several recent publications using existing satellite XCO_2 products.

- Schneising et al. (2013) presented an assessment of the satellite data over major anthropogenic CO_2 source regions. They used a multi-year SCIAMACHY XCO_2 data set and compared the regional XCO_2

enhancements and trends with the emission inventory EDGAR v4.2 (Olivier et al. 2012). They found no significant trend for the Rhine-Ruhr area in central Europe and the US East Coast but a significant increasing trend for the Yangtze River Delta in China of about 13 ± 8%/year, in agreement with EDGAR (10 ± 1%/year).

- Reuter et al. (2014b) studied co-located SCIAMACHY XCO_2 and NO_2 retrievals over major anthropogenic source regions. For East Asia they found increasing emissions of NO_x (+5.8%/year) and CO_2 (+9.8%/year), i.e., decreasing emissions of NO_x relative to CO_2 indicating that the recently installed and renewed technology in East Asia, such as power plants and transportation, is cleaner in terms of NO_x emissions than the old infrastructure, and roughly matches relative emission levels in North America and Europe.

- The higher resolution and continuous (if narrow) swath of OCO-2 has also enabled a range of plume inversion studies, focussed on the estimation of point source emissions of CO_2, e.g. Nassar et al. (2017), which have been extended to make use of co-located measurements of NO_2 from TROPOMI by Reuter et al. (2019) and Fuentes Andrade et al. (2023).

- Byrne et al. (2023) presented an ensemble-based product estimating national CO_2 budgets from 2015-2020 based on OCO-2 retrievals, in support of the Global Stocktake. This built upon a previous OCO-2 inversion intercomparison study by Crowell et al. (2019).

A series of studies have also addressed methane emissions.

- SCIAMACHY data have already been extensively used to improve our knowledge on regional methane emissions prior to the start of the GHG-CCI project (e.g., Bergamaschi et al. 2009). A more recent research focus was to shed light on the unexpected renewed atmospheric methane increase during 2007 and later years using ground-based and satellite data (e.g., Rigby et al. 2008, Dlugokencky et al. 2009, Bergamaschi et al. 2009, 2013, Schneising et al. 2011, Frankenberg et al. 2011, Sussmann et al. 2012, Crevoisier et al. 2013). Based on an analysis of SCIAMACHY year 2003-2009 retrievals an increase of 7-9 ppb/year (0.4-0.5%/year) has been found with the largest increases in the tropics and northern mid latitudes (Schneising et al. 2011) but a particular region responsible for the increase has not been identified (Schneising et al. 2011; Frankenberg et al. 2011). Bergamaschi et al. (2013) used SCIAMACHY retrievals and NOAA surface data for 2003-2010 and inverse modelling in order to attribute the observed increase of atmospheric concentrations to changes in emissions. They concluded that most of this increase is due to emissions in the Tropics and the mid-latitudes of the northern hemisphere, while no significant trend was derived for Arctic latitudes. The increase is mainly attributed to anthropogenic sources, superimposed with significant inter-annual variations of emissions from wetlands and biomass burning.

- The SCIAMACHY XCH_4 retrievals have also been used to improve chemistry-climate models (Shindell et al. 2013, Hayman et al. 2014).

- Methane emissions have also been obtained from GOSAT, as presented in a number of publications as shown in, e.g., Fraser et al. (2013, 2014), Monteil et al. (2013), Cressot et al. (2014), Alexe et al. (2015), Turner et al. (2015) and Pandey et al. (2016). Note that for these studies, often CH_4 retrievals from several satellites have been used (as well as NOAA data), e.g., Monteil et al. (2013), and Alexe et al. (2015) used SCIAMACHY and GOSAT retrievals and Cressot el al. (2014, 2016) used GOSAT, SCIAMACHY and IASI. Alexe et al. (2015) showed that the different satellite products resulted in relatively consistent spatial flux adjustment patterns, particularly across equatorial

	ESA Climate Change Initiative (CCI+)	Page 11
ghg cci (logo)	**Climate Assessment Report (CAR)** **for Climate Research Data Package 8 (CRDP#8)**	Version 1.0
	of the Essential Climate Variable (ECV) Greenhouse Gases (GHG)	8 February 2024

Africa and North America. Over North America, the satellite inversions result in a significant redistribution of emissions from North-East to South-Central USA, most likely due to natural gas production facilities.

- Several publications focused on (relatively localized) methane sources in the United States: For example, Schneising et al. (2014b) analyzed SCIAMACHY data over major US "fracking" areas and quantified methane emissions and leakage rates. For two of the fastest growing production regions in the US, the Bakken and Eagle Ford formations, they estimated that emissions increased by 990 ± 650 $ktCH_4$/year and 530 ± 330 $ktCH_4$/year between the periods 2006–2008 and 2009–2011. Relative to the respective increases in oil and gas production, these emission estimates correspond to leakages of 10.1% ± 7.3% and 9.1% ± 6.2% in terms of energy content, calling immediate climate benefit into question and indicating that current inventories likely underestimate the fugitive emissions from Bakken and Eagle Ford. Others also used SCIAMACHY data over the US to identify and quantify localized anthropogenic methane emission sources (Kort et al. 2014, Wecht et al. 2014). Last, Turner et al. (2015) used GOSAT retrievals within a meso-scale inversion system for the US.

- Such regional studies have been extended and expanded with the capabilities of TROPOMI, including studies focussing on basin-level oil and gas emissions of methane, including Schneising et al. (2020), and Zhang et al. (2020). This approach has been operationalized to provide weekly basin-level monitoring with the recent work of Varon et al. (2023).

- TROPOMI has also been used in recent studies to estimate national emissions, such as from China (Chen et al., 2022), and countries around the world (Shen et al., 2023).

- Recent publications have focussed on natural emisisons from the Tropics using GOSAT data, such as Parker et al. (2018), Lunt et al. (2019), Feng et al. (2022), and Yin et al. (2021), finding variability in Tropical emissions to be a driver of the recent methane growth rate.

- Many recent studies have exploited the high spatial resolution and broad coverage of TROPOMI measurements to identify and estimate the emissions from point source emissions of methane. A selection of such publications includes: Maasakkers et al. (2022), focussing on landfill emissions; Gao et al. (2023), assessing onshore oil and gas emissions; Lauvaux et al. (2022), focussing on oil and gas emissions; Maasakkers et al. (2021), quantifying emissions from a blow-out.

- Machine-learning methods have recently been applied by Balasus et al. (2023) to create a blended GOSAT+TROPOMI product, using the joint information to correct for retrieval biases.

- Regional inversions focussing on Eastern Asia by Liang et al. (2023) have found that inversions based on TROPOMI vs GOSAT data disagree on the distribution and magnitude of emissions across the region. Some of this difference is attributable to the difference in data coverage, with GOSAT measurements being comparatively sparse, but the lower methane emissions from the GOSAT inversions were also more consistent with surface- and aircraft-based inversions, suggesting some incongruity in the information between the two sensors.

For additional publications, see the publication list provided by the GHG-CCI+ website (https://climate.esa.int/en/projects/ghgs/publications/).

3. Assessment of satellite-derived XCO_2 products

3.1. Introduction

Given a decade of global inverse modelling studies assimilating real XCO_2 retrievals (since Basu et al., 2013, see Section 2), extended to 1.5 decades (Chevallier et al., 2005) in the case of partial column CO_2 retrievals, the current interest in XCO_2 products for global inverse modelling is about accurate multi-year global products. This has not been always the case (Chevallier et al, 2011). The first four GHG-CCI Climate Research Data Packages fulfilled this ambition with SCIAMACHY and TANSO retrievals.

The 5th, 6th, 7th and 8th GHG-CCI+ Climate Research Data Packages (CRDP#5, #6, #7 and #8, http://cci.esa.int/ghg#data) include three XCO_2 products from more recent satellite instruments with a similar ambition:

- CO2_TAN_OCFP (not updated in CRDP#8): retrieved from TanSat using University of Leicester's UoL-FP (or OCFP) algorithm
- CO2_OC2_FOCA: retrieved from OCO-2 using University of Bremen's FOCAL algorithm
- CO2_GO2_SRFP: retrieved from GOSAT-2 using SRON's RemoTeC (or SRFP) algorithm

The CRDP#8 version of the last two products is evaluated in this chapter within an inverse modelling framework. The first product, CO2_TAN_OCFP, has not been updated in CRDP#8. Comparisons are made with the surface air-sample-driven inversion and the satellite-driven inversion of the Copernicus Atmosphere Monitoring Service (https://atmosphere.copernicus.eu/, Chevallier, 2023a, 2023b). The latter assimilated latest version 11.1 of the official bias-corrected XCO_2 retrievals made by the NASA Atmospheric CO_2 Observations from Space (ACOS) algorithm described by Osterman et al. (2022).

The evaluated product from CRDP#8 is summarized in Table 1 below. The two CRDP#8 official bias-corrected products have been processed by LSCE on a GPU (Graphics Processing Unit) partition of the supercomputer Irene of http://www-hpc.cea.fr/en/complexe/tgcc.htm.

Product ID	Satellite	Algorithm	Data provider	Reference	Period available	Evaluators (sections)
CO2_OC2_FOCA	OCO-2	FOCAL, v10.1	IUP, Univ. Bremen	Reuter et al., 2017a, 2017b	09/2014-02/2022	LSCE (1.1, 0)
CO2_GO2_SRFP	GOSAT-2	SRFP, v2.0.2	SRON	Krisna et al., 2022a	02/2019-12/2021	LSCE (1.1, 0)

Table 1. XCO2 products evaluated in this report.

3.2.   Inversion method

The satellite data are assimilated alone, without combining them with other observations, in order to focus on their own signals. The much higher spatial resolution of the CO2_OC2_FOCA retrievals than the LMDz atmospheric transport model used here may cause numerical artifacts: to avoid them, we follow Crowell et al. (2019) by aggregating these retrievals in 10-second intervals, that roughly correspond to boxes of 67×10 km^2 for OCO-2, a surface area which is still much smaller than the individual grid boxes of $2.50^\circ \times 1.27^\circ$ of the model. This approach was also used in the CAMS OCO-2-driven inversion FT23r1 used here.

We use the two CRDP#8 XCO$_2$ products candidly, i.e. without modifying the retrieval values and their associated uncertainty in input to the inversion or, for CO2_OC2_FOCA, to the 10-s binning algorithm. However, if several 10-s-binned retrievals of a same orbit fall within the same model grid box, we inflate the variance of the retrieval errors by the number of concerned retrievals or 10-s-binned retrievals, in order to avoid likely local error correlations (at least from the transport model). We use the retrieval averaging kernels and prior profiles when assimilating them. As an example, processing the full multi-year series of CO2_OC2_FOCA within the inverse system required 10 days of computation on 9 GPUs.

The fluxes inferred from CO2_OC2_FOCA and CO2_GO2_SRFP are compared to two benchmark inversion: the CAMS official inversion products v22r1 that exclusively assimilated surface air-sample measurements at 159 sites from the Global Atmosphere Watch programme, and the CAMS official inversion product FT23r1 that exclusively assimilated the ACOS OCO-2 v11.1 retrievals over land. Ocean glint retrievals were not assimilated in FT23r1 because of likely systematic errors (Chevallier et al., 2019), but such a selection is not done for the CRDP#8 products here in the absence of similar evidence. Actually, for CRDP#7, we made a test without the ocean data of CO2_OC2_FOCA, but results were found less realistic than with these (Chevallier and Marshall, 2023).

The inversion system works at the grid-point weekly scale and generates a large volume of data. The present comparison focuses on a few key quantities: (i) the global annual growth rate that is well known from the NOAA marine surface data (Conway et al. 1994, http://www.esrl.noaa.gov/gmd/ccgg/trends/global.html), (ii) the grid-point annual-total fluxes, (iii) zonal annual CO$_2$ budgets, (iv) the model-equivalent to upper-air measurements.

3.3.   Global annual atmospheric growth rates

In 2019, the Inverse modelling protocol for the annual global carbon budget of the Global Carbon Project (GCP) started to use a quality criterion on the global annual atmospheric growth rate of the inversion (Chevallier et al. 2019, 2020, 2021, 2022, 2023): "using a conversion factor, the series of annual fluxes will be compared to the annual trend of globally-averaged marine measurements

	ESA Climate Change Initiative (CCI+)	Page 14
ghg cci	**Climate Assessment Report (CAR)** for Climate Research Data Package 8 (CRDP#8)	Version 1.0
	of the Essential Climate Variable (ECV) Greenhouse Gases (GHG)	8 February 2024

(http://www.esrl.noaa.gov/gmd/ccgg/trends/). Submissions that show notably different interannual variations will be excluded."

The OCO-2 Science team's Model Intercomparison Project v10 (MIPv10) adopted a selection criterion on the mean growth rate for the inversion products it gathered for the Global Stocktake (Byrne et al., 2023): it required the selected inversions to have a 6-year growth rate over 2015-2020 equal to 2.54 ± 0.08 ppm/a, based on NOAA's reference estimate (Brendan Byrne, personal communication, 4 January 2022). This criterion is quantitative, in contrast to the GCP one, but it is limited to the mean value: it just checks that the model simulation does not diverge over time.

In all previous CARs, poor inversion results were associated to poor inversion annual growth rates in terms of bias and/or standard deviation.

Over the seven full years 2015-2021, the CAMS satellite inversion FT23r1 fits NOAA's numbers (as of 5 August 2023) with a bias of -0.02 ppm/a and a standard deviation of 0.07 ppm/a [1]. Its surface-driven counterpart (v22r1) shows a smaller bias and a larger standard deviation: 0.01 ± 0.14 ppm/a [2]. The FOCAL-driven inversion is at 0.00 ± 0.28 ppm/a. The fit is worse than with the FOCAL version of the previous CRDP (0.03± 0.23 ppm for 2015-2020 in CRDP#7 vs. +0.06 ± 0.26 ppm here for the same period). With a mean growth rate over 2015-2020 equal to 2.59 ppm/a, the FOCAL inversion passes the MIPv10 6-year growth-rate criterion, like the CAMS satellite inversion FT23r1 (with a value of 2.55 ppm/a).

For the SRFP-driven inversion, we consider the two full years 2020 and 2021 (knowing that the retrieval product does not allow any spin-down for the second one). NOAA's value for the growth rate is of 2.34 and 2.47 ppm/a, respectively. The SRFP-driven inversion says 2.64 and 2.28 ppm/a. The year with the best fit is actually the one without spin-down, therefore the less reliable one. In any case, it is still 0.19 ppm/a far from NOAA's reference estimate. The CAMS satellite inversion FT23r1 is much closer to the NOAA value with 2.35 ppm/a and 2.49 ppm/a, respectively.

3.4. Maps of annual budgets

Figure 1 display the maps of the inferred annual budgets of natural CO_2 fluxes for year 2020 that is included in the two CRDP products considered here. The figures also display the maps for the two CAMS inversions. As shown already by Chevallier et al. (2019), the two CAMS inversions have comparable flux patterns in the northern extra-Tropics, but the ACOS-driven inversion has more spatial gradients than the surface-driven one in the Tropical lands where the surface measurement network is particularly sparse. The two CRDP#8-driven inversions have even larger gradients there (Australia excepted), but also in the northern extra-Tropics. The colour bar has actually not been adapted to their variability. Surprisingly, many spatial patterns (irrespective of their amplitude) are

---

[1] We assume a conversion factor of 2.086 GtC·ppm^{-1}, from Prather (2012), which may be slightly different from other studies.
[2] Note that the NOAA estimate and the surface-driven CAMS one are not independent since the surface-driven CAMS inversion assimilates the individual NOAA measurements

	ESA Climate Change Initiative (CCI+)	Page 15
ghg cci	**Climate Assessment Report (CAR)** for Climate Research Data Package 8 (CRDP#8)	Version 1.0
	of the Essential Climate Variable (ECV) Greenhouse Gases (GHG)	8 February 2024

similar between the three satellite-driven inversions over land. Over the ocean, the four inversions show significant differences in the spread of outgassing regions: the two OCO-2 driven inversions (right column) reduces it compared to the air-sample driven inversion (top left) while the GOSAT-2-driven inversion enlarges them (bottom left). None of the maps seems unrealistic, which was not the case with CRDP#7 (Chevallier and Marshall, 2023).
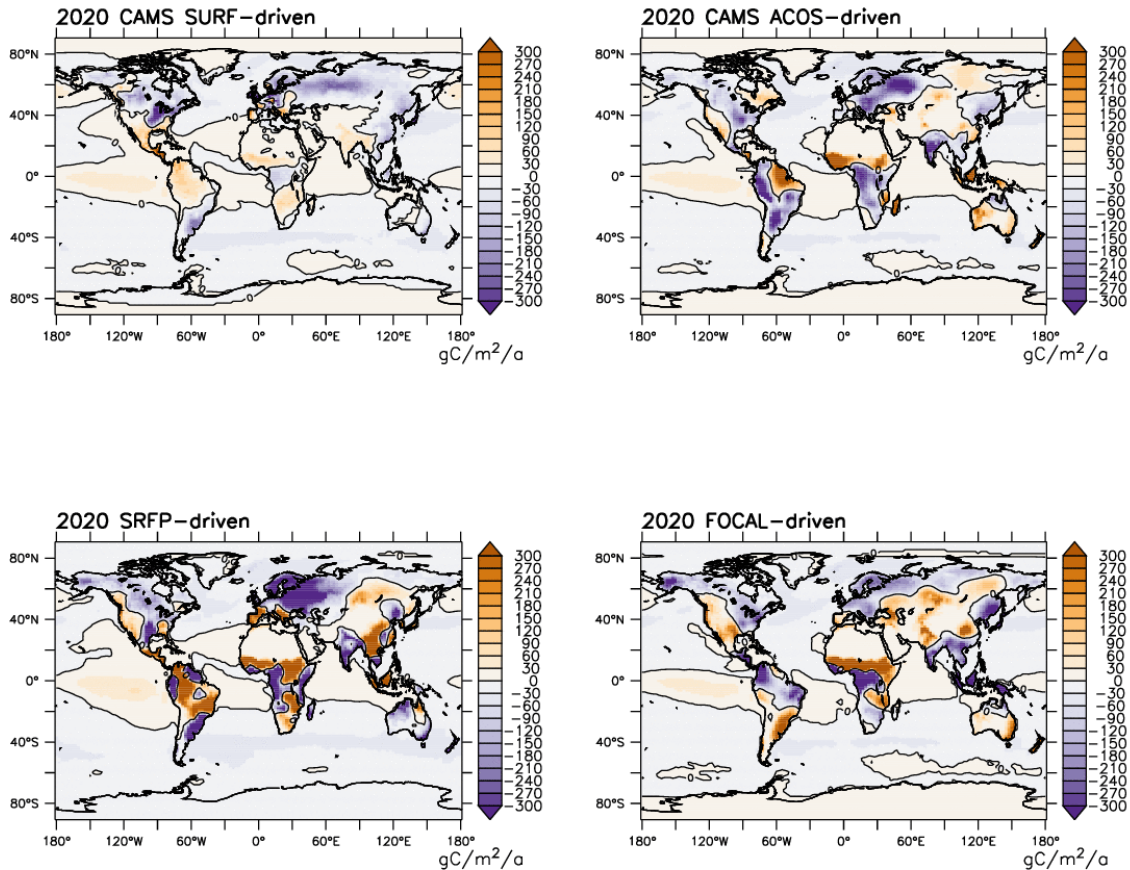

Figure 1. Grid-point annual budget of the natural CO_2 fluxes for year 2020, for the two CAMS inversions, for the FOCAL inversion and for the SRFP inversion. In the sign convention, positive fluxes correspond to a net carbon source into the atmosphere.

3.5. Annual budget time series

The time series of the annual natural carbon budgets at several very broad scales are displayed in Figure 2 for the period between 2015 and 2021 for the two CAMS inversions and for the CO2_OC2_FOCA one: the globe, the northern or southern extra-Tropics, and the Tropics with lands and oceans either separated or combined. At the global scale (top row), the curves reflect the growth rate discussed in Section 3.3, but without the fossil fuel and cement flux component: recognize the

larger variability of CO2_OC2_FOCA. The CAMS ACOS inversion remains close to the CAMS surface inversion in all subplots, which is less the case for the CO2_OC2_FOCA inversion.

The two CAMS inversions locate the land sink mostly in the northern extra-Tropics in contrast to the CO2_OC2_FOCA one that locates it mostly in the Tropics (middle row). In all three, a large year-to-year variability is seen in the Tropics. The southern extra-Tropical lands (that represent a relatively small surface area) are close to neutral each year, or slightly emissive (CO2_OC2_FOCA).

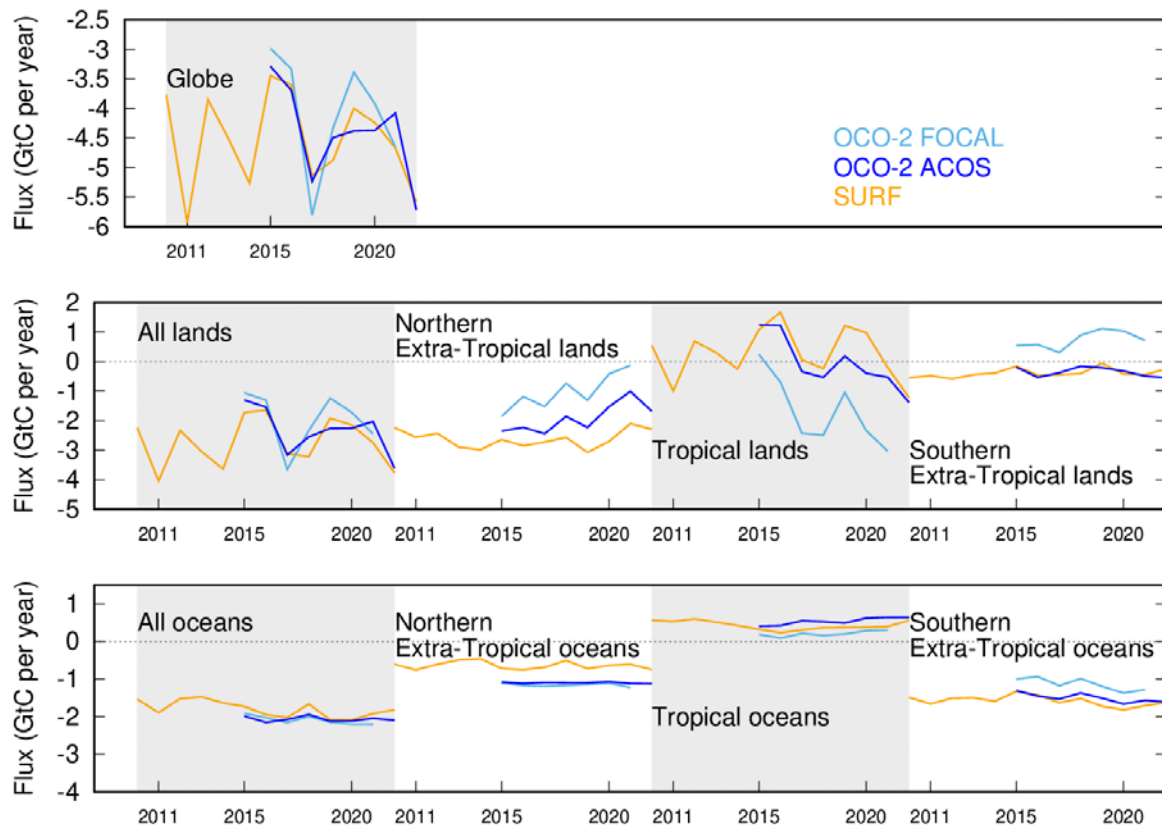The ocean sink latitudinal distribution inferred from the three inversions is comparable (bottom row).

Figure 2. Inferred natural CO$_2$ annual flux (without fossil fuel emissions) averaged over the globe or over all lands or oceans. In the case of lands and oceans, three broad latitude bands are also defined: northern extra-Tropics (north of 25°N), Tropics (within 25° of the Equator), and southern extra-Tropics (south of 25°S). The blue and orange curves correspond to the CAMS surface-driven (SURF) and OCO-2-driven (ACOS) products. In the sign convention, positive fluxes correspond to a net carbon source into the atmosphere.

	ESA Climate Change Initiative (CCI+)	Page 17
![ghg cci logo]	**Climate Assessment Report (CAR)** **for Climate Research Data Package 8 (CRDP#8)**	Version 1.0
	of the Essential Climate Variable (ECV) **Greenhouse Gases (GHG)**	8 February 2024

3.6.   Fit to unassimilated upper-air measurements

Following the approach defined in Chevallier et al. (2019) and applied in GCP's Global Carbon Budget since then (see, e.g., Figure B4 of Friedlingstein et al. 2022), we now focus on the dry air mole fraction measurements made by aircraft and Aircore devices in the free troposphere. The free troposphere is simply defined here as the atmospheric layer between 2 and 7 km above sea level. The measurements are here from NOAA's ObsPack Globalview+_v8.0 and ObsPack NRT_8.1 for the period January 2015 – December 2022.
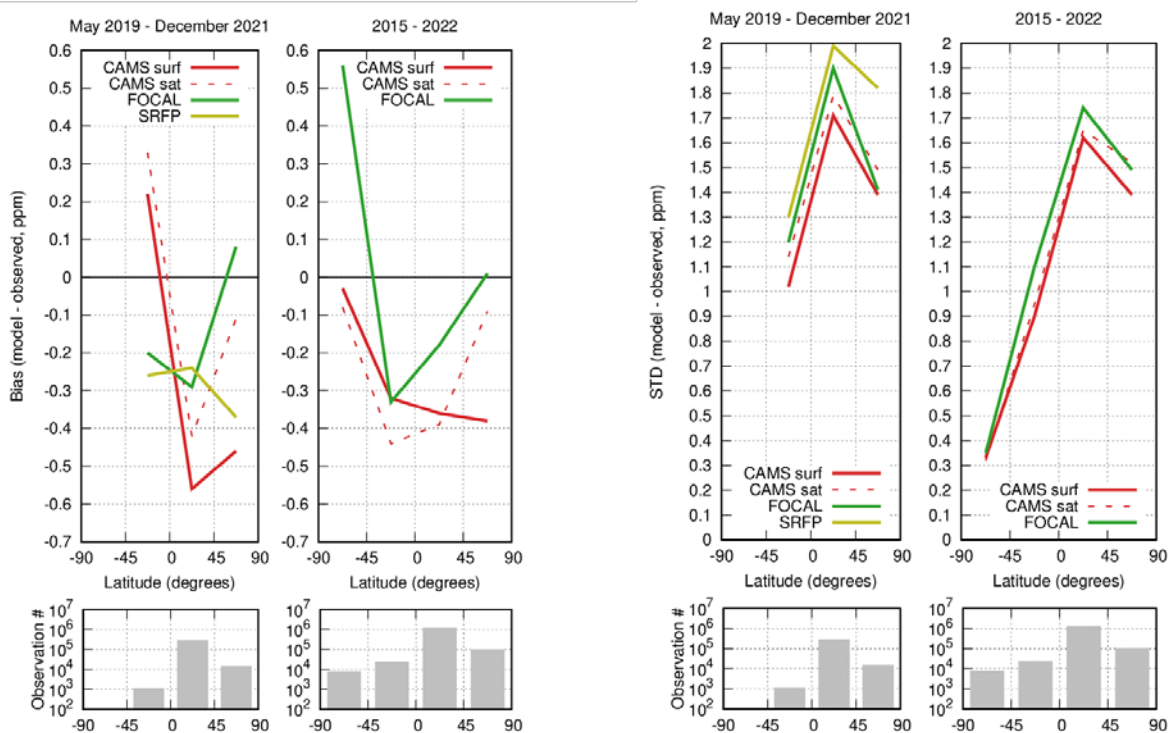

Figure 3. The mean (left) and standard deviation (STD, right) of the model minus observations is shown for four latitude bands in two periods: May 2019 – December 2021 and years 2015 – 2022. The four inversions (three only for the second period) are compared to independent CO₂ measurements made aboard aircraft or Aircore devices over many areas of the world between 2 and 7 km above sea level. Aircraft and Aircore measurements archived in NOAA's ObsPack Globalview+_v8.0 and ObsPack NRT_8.1 have been used to compute the statistics of the differences in four 45° latitude bins. Land and ocean data are used without distinction, and observation density varies strongly with latitude and time, as seen in the lower panels. Adapted and extended from Friedlingstein et al. (2022).

The model values are strikingly different from the upper-air measurement for none of the four inversions. The FOCAL inversion exceeds the symbolic 0.5 ppm bias threshold for the May 2019 – December 2021 period, in contrast to the other ones, but all biases are overall comparable to those of the inversions selected by the GCP (Figure B4 of Friedlingstein et al. 2022). In terms of standard deviation, we note that the CAMS air-sample driven inversion displays the smallest ones for the two periods, followed by the CAMS ACOS-driven one, the FOCAL-driven one and finally, for its period, the SRFP-driven inversion.

3.7.   Conclusions

The assimilation of the CRDP#8 products in the CAMS/LSCE global inversion system infers a latitudinal distribution of CO_2 surface fluxes that is very different from that obtained by both the assimilation of surface air-sample measurements and the assimilation of NASA's retrievals from OCO-2. We think that it is less credible because it yields a poorer simulation of the atmospheric growth rate and a poorer fit to independent atmospheric measurements.

The consistent results obtained in the CAMS inversions between the surface air-sample measurements and the ACOS retrievals demonstrates that there is no fundamental limitation in atmospheric inverse modelling (e.g., in the realism of the transport model or in the modelled error statistics) when assimilating satellite XCO_2 retrievals. The ACOS-driven CO_2 surface fluxes have actually been part of the official CAMS data portfolio since year 2019 and several ACOS-driven inversions pass the quality control of GCP's Global Carbon Budget (Friedlingstein et al. 2022).

ACOS and CO2_OC2_FOCA exploit the same OCO-2 spectra. The various tests performed do not allow us to identify the distinctive asset of ACOS in our system: the data precision (that seem to be better for ACOS according to the reported uncertainty of each product), the data trueness (linked to the quality of the physical retrieval scheme and to its empirical bias-correction), the accuracy of the averaging kernels (see Chevallier, 2015, for a discussion on potential issues with the averaging kernel profiles), or a combination of these qualities at once. These hypotheses implictely involve the retrieval quality control. Detailed sensitivity tests could be performed for this, but note that our single CO2_OC2_FOCA-driven inversion already represented a large computational effort that lasted ten days on a supercomputer.

For CO2_GO2_SRFP, we note that so far GOSAT-driven inversions have not reach the quality of OCO-2 driven ones to our best knowledge, and we may meet such a limitation with GOSAT-2 as well, due to the instrument quality joined to its sampling strategy. However, even with this challenge in mind, the simulation of the atmospheric growth rate still seems to be particularly poor.

About computational effort, CO2_OC2_FOCA's distinct advantage compared to ACOS is its representation of multiple scattering effects in the radiative transfer in a form that is not costlier than absorption. In preparation for the Copernicus CO_2 Monitoring Mission that will provide even larger amount of data than OCO-2 (Pinty et al., 2017), the processing of the OCO-2 archive, which is very large by today's standards, by CO2_OC2_FOCA represents an important achievement. In this context and resources permitting, it would be important to document their performance in more detail in order to help prioritize future developments.

4. Assessment of satellite-derived XCH$_4$ data products

4.1. Introduction

Global methane inversions based on satellite measurements are already long established, going back to the initial SCIAMACHY XCH$_4$ dataset from 2003, followed by over a decade of soundings from GOSAT, with improved stability and measurement precision, but sparser data coverage. With the launch of Sentinel-5 Precursor (S5P) in October 2017, these measurements moved from experimental measurements to an operational product, with vastly increased data density through a small footprint (7-km at nadir) and a continuous wide swath (2600 km). A year later, in October 2018, the Japanese satellite GOSAT-2 was launched, the successor to the successful GOSAT mission.

The 8th GHG-CCI+ Climate Research Data Package (CRDP#8, https://climate.esa.int/en/projects/ghgs/#data) includes the following three CH$_4$ products, resulting from these two sensors:

- CH4_S5P_WFMD: retrieved from TROPOMI on S5P using the University of Bremen's WFMD algorithm
- CH4_GO2_SRFP: retrieved from GOSAT-2 using SRON's full physics RemoTeC algorithm
- CH4_GO2_SRPR: from GOSAT-2 using SRON's proxy RemoTeC algorithm, retrieving the ratio of CH$_4$ to CO$_2$

Product ID	Instrument	Algorithm	Data provider	Reference	Period available	Evaluators (sections)
CH4_S5P_WFMD	TROPOMI	WFMD, v1.8	IUP, Univ. Bremen	Schneising et al., 2019	11/2017-05/2023	DLR (4.2-4.5)
CH4_GO2_SRFP	GOSAT-2	V2.0.2	SRON	Krisna et al., 2022a	02/2019-12/2021	DLR (4.2-4.5)
CH4_GO2_SRPR	GOSAT-2	V2.0.2	SRON	Krisna et al., 2022b	02/2019-12/2021	DLR (4.2-4.5)
CH4_S5P_SRON	TROPOMI	RemoTeC 2.5.0	SRON	Hu et al., 2016; Lorente et al., 2021	04/2018-08/2023	DLR (4.2-4.5)

Table 2: XCH$_4$ products evaluated in this report. Only the first three are officially members of CRDP#8, but the operational SRON retrievals of S5P measurements is included for context and completeness.

The GOSAT-2 retrievals are now available from February 2019 through the end of 2021, providing more than two full years of data and allowing for their inclusion in inversion intercomparisons for the first time.

	ESA Climate Change Initiative (CCI+)	Page 20
ghg cci	**Climate Assessment Report (CAR)** for Climate Research Data Package 8 (CRDP#8)	Version 1.0
	of the Essential Climate Variable (ECV) Greenhouse Gases (GHG)	8 February 2024

To enrich the comparison, the operational retrieval of XCH_4 from S5P (Hu et al., 2016, with updates described in Lorente et al., 2021) is also included in the analysis, and is referred to as CH4_S5P_SRON in the text. The evaluated XCH_4 products are summarized in Table 2.

4.2. Preprocessing of satellite retrievals
4.2.1. Method

In this section we begin by plotting the data products themselves, to get a view of the temporal and spatial distribution, and assess the data coverage when aggregated onto the spatial grid of the global transport model used in the inversion. We then compare the different satellite products with concentration fields resulting from a forward simulation of the TM3 transport model (Heimann and Körner, 2003) using optimized fluxes from an inversion assimilating flask measurements from 91 surface sites, using data provided by the ObsPack v5.1 release up to the end of 2021, and the ObsPack NRT v5.1 release for more recent measurements (Schindt et al., 2023a and 2023b). The inversion was carried out using the Jena CarboScope variational inversion system (based on Rödenbeck et al., 2003). The transport is carried out at 3.8° latitude by 5° longitude resolution and with 19 vertical levels, and is driven by meteorological fields from the ERA5 reanalysis.

Because the model transport is imperfect, especially with respect to the tropopause height and the gradient of methane within the stratosphere, the comparison to the surface-optimized fields is used to derive a model-specific bias correction. The bias correction is modelled as a 2nd order polynomial as a function of latitude and month, following the approach of Bergamaschi et al. (2007) (see Equation 4 from this paper). Because this correction is independent of longitude, the information about local gradients is largely maintained, while ensuring that the model can simultaneously interpret total-column and surface-based measurements of CH_4 in a consistent manner.

When comparing the modelled XCH_4 columns to the XCH_4 measurements, both the prior profile and the averaging kernel are taken into account. Because the spatial resolution of the S5P measurements is so much higher than that of the model fields, we average them to create super-observations for use in the inversion. In CAR7, this was done in the following manner:

- Count all retrievals with quality flag "good" (or, for CH4_S5P_SRON, those with qa filter > 0.5) that fall within a model doxel (gridbox per orbit)
- Average the XCH_4 values, weighted by the inverse of measurement precision
- Calculate the mean averaging kernel, averaging per retrieval layer, weighted by the inverse of the measurement precision
- Determine the super-obs measurement precision, as the maximum of:
  - a) Double the weighted mean precision or
  - b) The standard deviation of the XCH_4 measurements in the doxel

Choosing the maximum between the doubled weighted mean reported precision from the retrieval product and the standard deviation of the soundings within the doxel was intended to balance the

	ESA Climate Change Initiative (CCI+)	Page 21
ghg cci	**Climate Assessment Report (CAR)** for Climate Research Data Package 8 (CRDP#8)	Version 1.0
	of the Essential Climate Variable (ECV) Greenhouse Gases (GHG)	8 February 2024

very different reported precision of the TROPOMI retrievals from WFMD vs. the two SRON products, but resulted in overinflating the WFMD errors, which are of a reasonable magnitude as reported. This is discussed in more detail in Section 4.2.2, and the method used is summarized in Table 3.

4.2.2. Data coverage and creation of super-observations

TROPOMI: The spatial coverage of the S5P satellite retrievals are shown for January 2020 in Figure 4. Compared to the previous SRON operational retrieval, the difference in the number of good soundings between the two products is not as stark. Nonetheless, it can be seen that the WFMD retrieval has more retrievals that pass the quality filtering, both over land and over the ocean, a pattern which is consistent for the full measurement period. This is particularly notable for some areas, such as mountainous regions (e.g. the Andes and the Himalayas), and at very high latitudes, as the cut-off solar zenith angle is different between the two products (70° for SRON, 75° for WFMD).

It should be noted that the gap in data coverage in the operational SRON product documented in CAR7 has been removed. This gap was due to a lack of VIIRS data, which were used for cloud screening. The newest version of the operational retrieval has used an AI-based method, trained on scenes when VIIRS data were available, to screen for clouds based only on the information in the S5P radiances, thus improving the data coverage.

The mean concentrations are generally very similar, though it can be seen that there are more extremely high values in the SRON product for this month (e.g. over central Africa). At first glance the TROPOMI retrievals appear quite similar, at least the structures that are captured are the same.
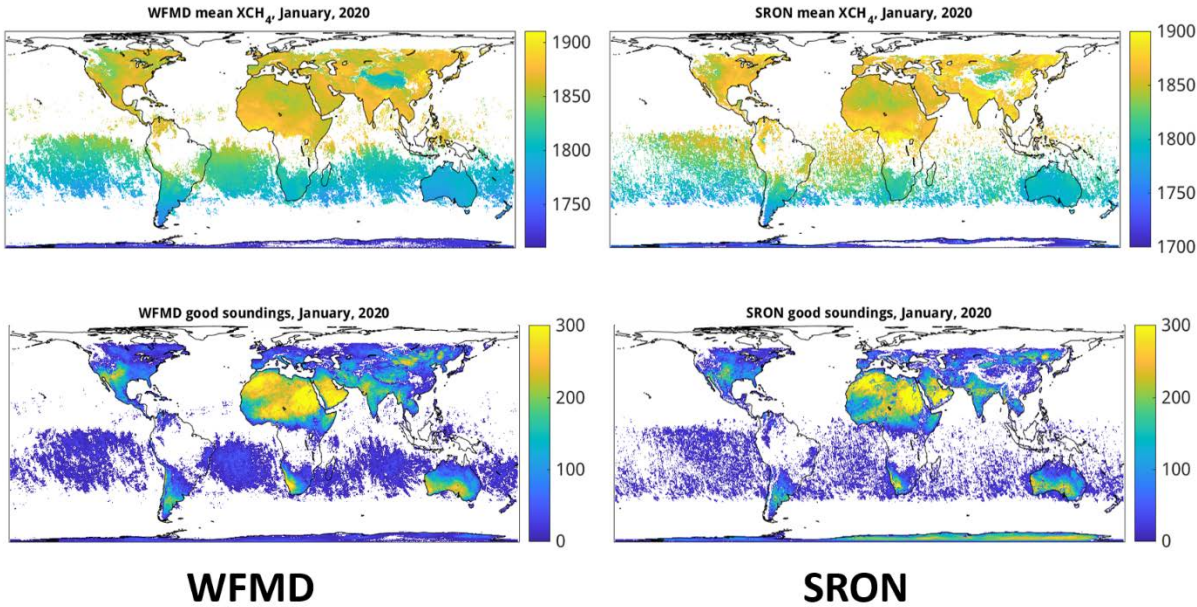

Figure 4: TROPOMI XCH$_4$ retrievals from the WFMD (left) and SRON (right) products for January, 2020, averaged onto 0.25° x 0.25° bins. The mean XCH4 values are shown in the top row, and the number of good soundings per bin are shownin the bottom row.

As discussed in Section 4.2.1, these soundings were then aggregated onto the grid resolution of the global transport model to produce super-observations. This has been done in the production of previous CARs as well, and a previous error in this processing was identified and amended. Because the error is relevant in terms of how the data are distributed to users, the details are described here. Despite the fact that the WFMD dataset systematically reports more retrievals that pass the quality filter, when aggregated onto the superobs grid, this did not appear to be the case (see Figure 5).

This was entirely the result of user error: because the (very easy to use, and much-appreciated) GHG-CCI data format stores the retrievals by day, rather than orbit (which is how the operational SRON retrievals are stored). This led to an error in the script that prepared the suberobs, as all soundings per day were initially aggregated, rather than per orbit. Especially at higher latitudes, this can lead to a large difference in the number of independent superobs that are then assimilated into the model.

Once identified, this error was easily corrected. It is still mentioned explicitly here, as the orbit number was not reported in the CRDP files for the GOSAT-2 retrievals. Thus, the CAR recommends that the orbit number should be added to these files, and any future GHG-CCI products.
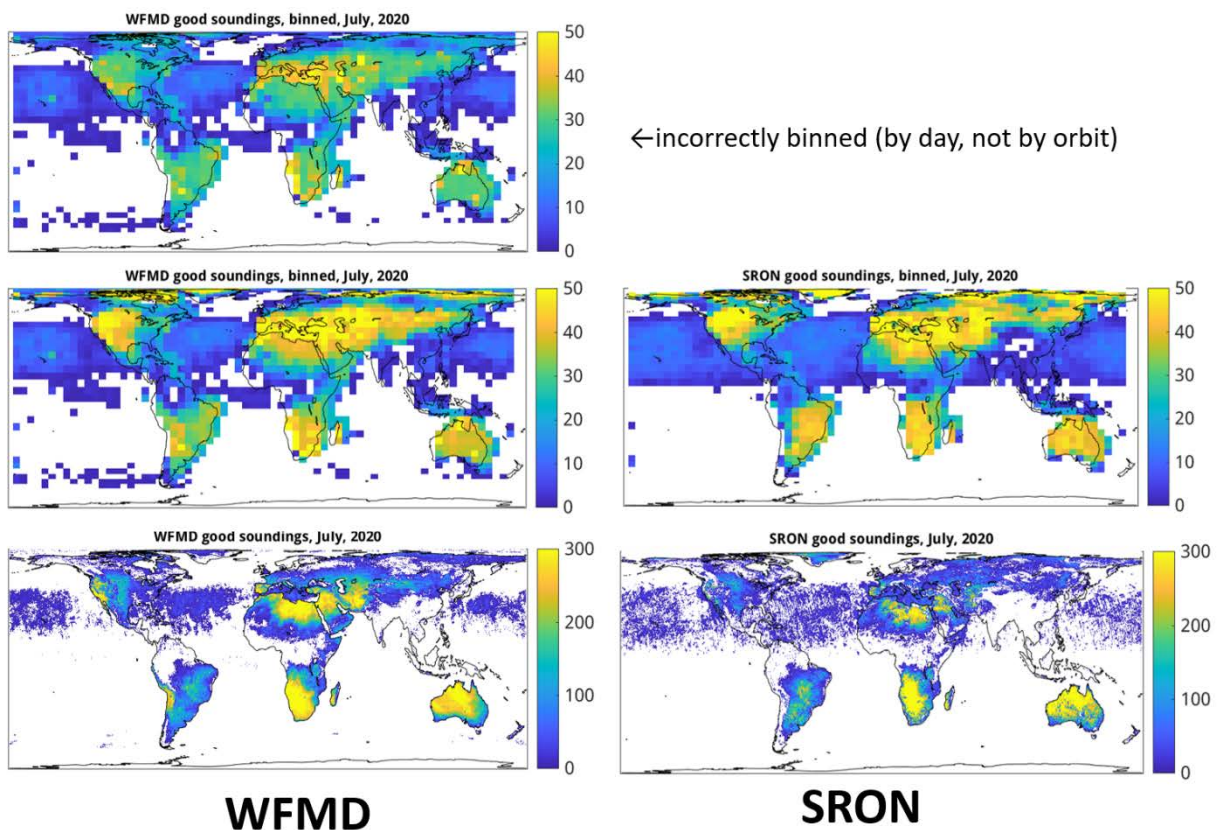

Figure 5: Number of good soundings for July, 2020 for WFMD (left) and SRON (right). The number of good superobs for the same month are shown aggregated onto the TM3 grid in the middle row, while the number based on incorrect aggregation for WFMD is shown in the top row.

	ESA Climate Change Initiative (CCI+)	Page 23
![ghg cci logo]	**Climate Assessment Report (CAR)** **for Climate Research Data Package 8 (CRDP#8)**	Version 1.0
	of the Essential Climate Variable (ECV) **Greenhouse Gases (GHG)**	8 February 2024

The next step in creating the superobs is to consider the uncertainties that should be used. Here we start by comparing the errors as reported in the data products, which are shown in Figure 6. While the shape of the zonally-averaged XCH_4 and its reported uncertainty are similar between the two products, the reported uncertainties for the SRON retrievals are approximately five times smaller than those reported for WFMD. The very low uncertainties are not consistent with comparisons between the retrievals and TCCON measurements, which is what motivated the proposed error inflation for the superobs described in Section 4.2.1.
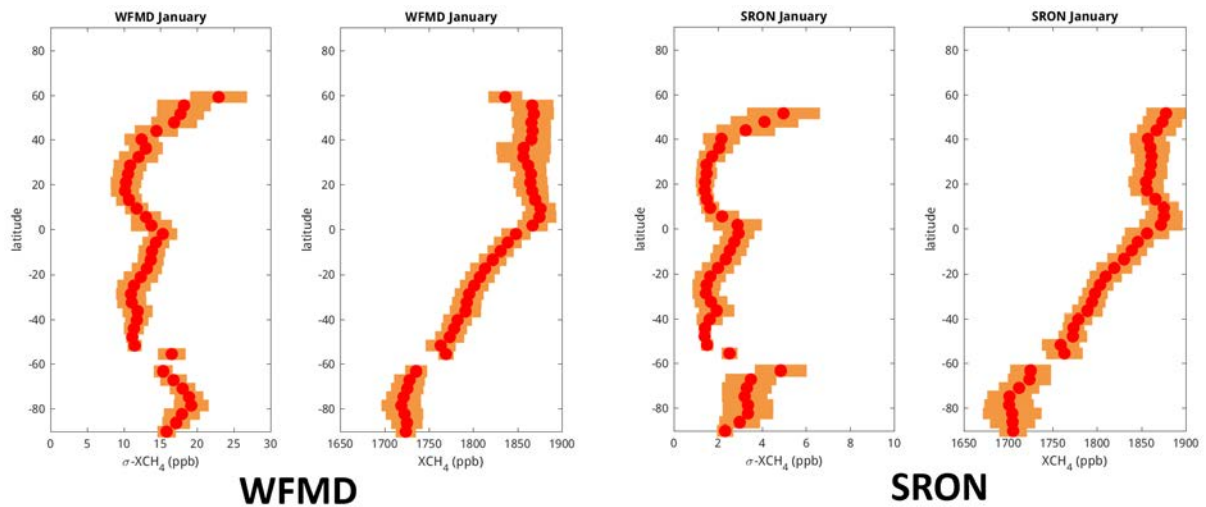

Figure 6: Mean (in red) and standard deviation (in red) of the zonally-averaged XCH_4 uncertainty and XCH_4 reported in the WFMD (two left panels) and SRON (two right panels) data products. While similar in shape, the reported uncertainties in the SRON product are approximately five times smaller than those reported by WFMD.
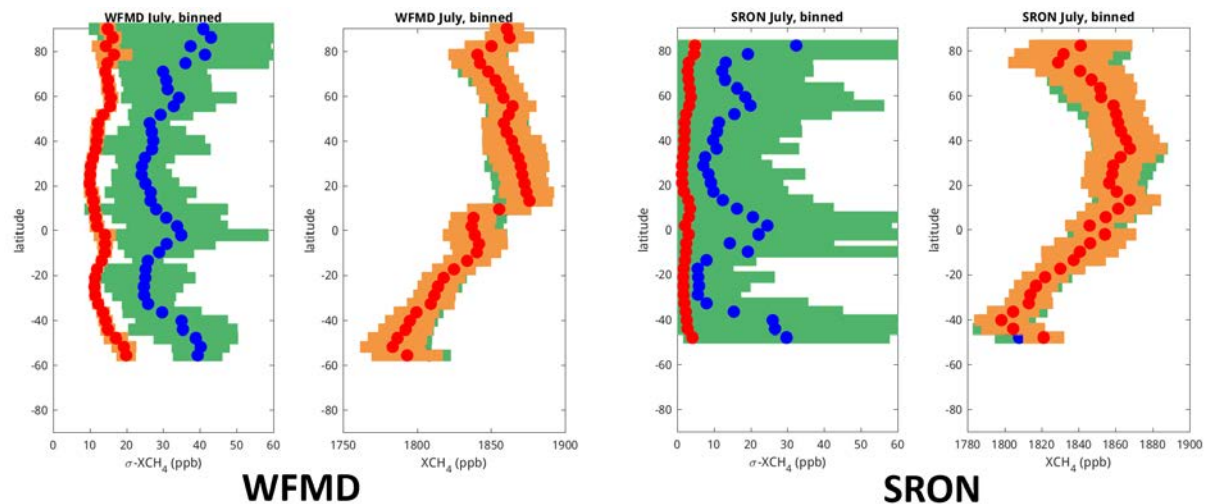

Figure 7: The red and orange curves are the same as those in Figure 6. The inflated errors based on the first method described in Section 4.2.1 are shown in blue (mean) and green (standard deviation).

	ESA Climate Change Initiative (CCI+)	Page 24
ghg cci	**Climate Assessment Report (CAR)** for Climate Research Data Package 8 (CRDP#8)	Version 1.0
	of the Essential Climate Variable (ECV) Greenhouse Gases (GHG)	8 February 2024

However, when comparing the inflated errors (mean and standard deviation shown in blue and green, respectively) in Figure 7, it is clear that the WFMD errors are essentially always based on doubling the reported errors, whereas the SRON errors are taken as the standard deviation within the doxel. This leads to an overestimation of the WFMD errors that would be used in the inversion. As such, the procedure for getting the measurement uncertainties of the WFMD superobs no longer doubles the mean reported precision. The difference in these two approaches is summarized in Table 3.

TROPOMI retrieval	CH4_S5P_WFMD	CH4_S5P_SRON
The maximum of:	The weighted mean of the reported measurement uncertainty	Double the weighted mean of the reported measurement uncertainty
	The standard deviation of all XCH_4 measurements in the doxel	The standard deviation of all XCH_4 measurements in the doxel

Table 3: Overview of the method for calculating the measurement uncertainty of the aggregated superobs used in the inversion.

GOSAT-2: The data coverage for the proxy and full-physics retrievals for GOSAT-2 (CH4_GO2_SRPR and CH4_GO2_SRFP, respectively) are shown in Figure 8. As expected, the proxy product (CH4_GO2_SRPR) has more measurements and thus, more coverage, than the full-physics retrieval (CH4_GO2_SRFP). Because these data are comparatively sparse, they are assimilated individually, and superobservations are not used. The number of good soundings at model resolution is shown only for comparability with the WFMD data coverage shown in Figure 5.

Bias correction: As introduced in Section 4.2.1, a 2nd-degree polynomial was fit to describe the mismatch between the XCH_4 retrievals and optimized model fields based on surface measurements only.

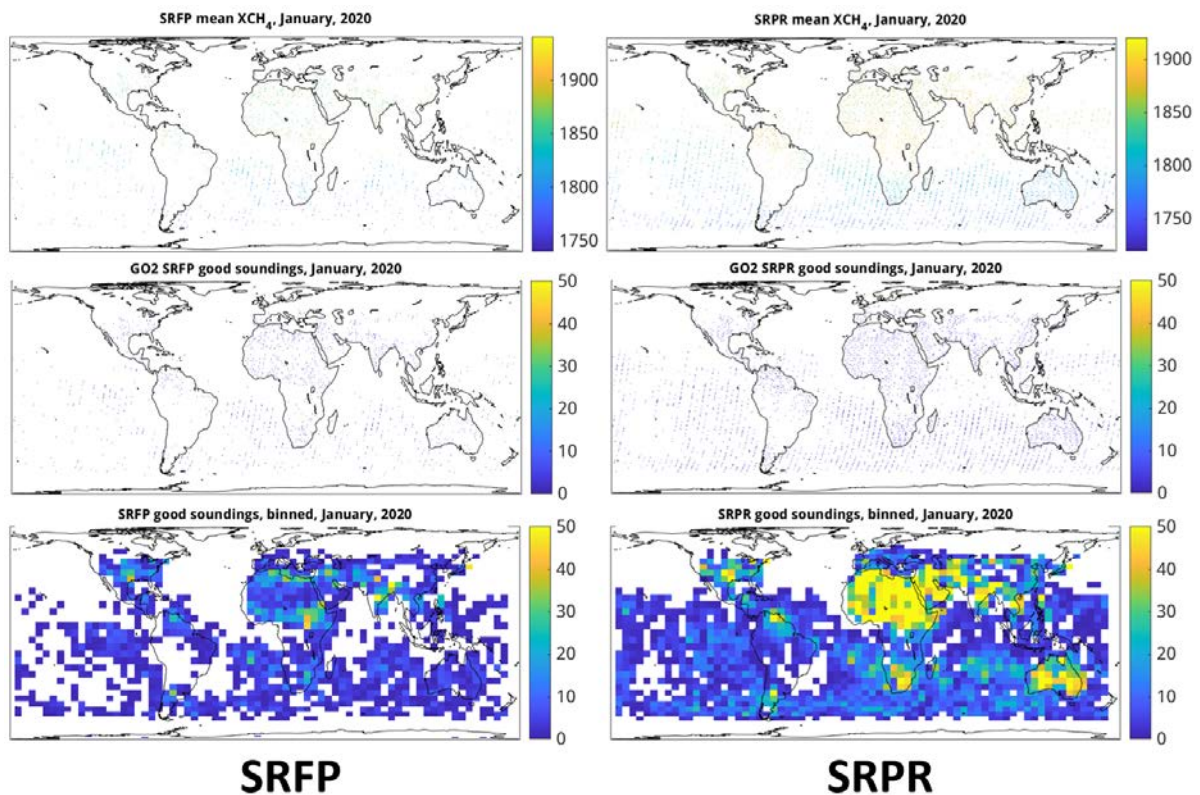|	ESA Climate Change Initiative (CCI+)	Page 25
ghg cci	**Climate Assessment Report (CAR)** for Climate Research Data Package 8 (CRDP#8)	Version 1.0
	of the Essential Climate Variable (ECV) Greenhouse Gases (GHG)	8 February 2024

Figure 8: Mean XCH$_4$ values binned at 0.25° x 0.25° resolution (top row) for January, 2020, for the GOSAT-2 retrieval products CH4_GO2_SRFP (left) and CH4_GO2_SRPR (right), with the number of good soundings per bin (middle row). The bottom row shows the number of good soundings over the month when aggregated onto the spatial grid of the global model.

4.3. Methane inversion experiments with the Jena CarboScope

After applying the bias corrections to the measurements, aggregated into super-observations, the two TROPOMI XCH$_4$ retrieval products and the two GOSAT-2 products were assimilated into the Jena CarboScope inversion system to attain optimized fluxes. The satellite data were assimilated alone, without combining them with other observations, in order to focus on the signals inherent to the measurements. From a scientific point of view this may not be the optimal approach: including continuous high-precision surface measurements can have a stabilizing effect on the results. However, it can be difficult to simultaneously assimilate both due to inconsistencies in the information content even after model-specific bias correction. Because the goal of this assessment is to examine the retrieval products on their own merit, it was decided not to combined the data streams, but rather keep them separate. The Jena CarboScope system is a variational inversion system, optimizing for the total methane fluxes, based on prior fluxes from bottom-up inventories and process models. The fluxes are optimized on a grid cell level, with category-based correlation lengths in space and time.

	ESA Climate Change Initiative (CCI+)	Page 26
ghg cci	**Climate Assessment Report (CAR)** for Climate Research Data Package 8 (CRDP#8)	Version 1.0
	of the Essential Climate Variable (ECV) Greenhouse Gases (GHG)	8 February 2024

The fluxes inferred from these satellite inversions are compared to the inversion over the same time period using the 91 flask sites, as described previously. This constitutes almost three times the number of surface stations that were used in the methane assessment for CAR7.

4.4. Global mean atmospheric mixing ratio and growth rate

Similar to the approach for CO_2 in Section 3.3, the results from the inversions are compared to global estimates derived directly from the flask measurements. In this case, two estimates are used: NOAA estimates the monthly mean global concentration of methane near the surface based on measurements from its network of marine boundary layer sites (Lan et al., 2022; https://gml.noaa.gov/ccgg/trends_ch4/). Similarly, the World Data Centre for Greenhouse Gas Measurements (WDCGG) provides a similar monthly measurement based on near-surface measurements, but includes more continental sites in their estimate, which leads to slightly higher estimates than NOAA's. The WDCGG estimates are reported in the annual WMO Greenhouse Gas Bulletin, and are regularly updated on the WDCGG website (https://gaw.kishou.go.jp/publications/global_mean_mole_fractions). Given the short time period available for the CRDP methane datasets being considered in the CAR, an analysis of monthly concentrations is attractive, even though we would expect this quantity to be less robust than an annual value.

To compare these to the optimized fields resulting from the inversion of the different products, the mean methane mixing ratio for each month is taken, averaged at the lowest model level over the whole globe, weighted by the area of the gridbox. The result of this comparison is shown in Figure 9. For reference, the concentrations resulting from the prior flux are included as well.

It is immediately clear that the trend in the prior is negative, whereas all the data-based inversion managed to capture the growth rate found in the NOAA and WDCGG estimates derived directly from station data. (The anomalies at the very start of 2018 should be ignored, as spin-up effects with sparse data coverage.) It can be seen that the two TROPOMI-based inversions agree quite well with one another, and the two GOSAT-2-based inversions agree quite well with one another, though the absolute difference between them is substantial. Indeed, the GOSAT-2 retrievals are lower than the NOAA value, which represents the marine background sites. This is unexpected, and suggests a low bias.

In terms of magnitude, the TROPOMI-based inversions are much closer to the surface-based inversion, though without as much variabilitiy in the seasonal cycle, which may reflect differences in measurement coverage over the year. Compared to the previous version of the CAR, the surface-based inversion has amuch noisier seasonal cycle: this is related to the the substantially larger station set that was used, and may reflect over-fitting of stations that cannot be represented well by the global model. The GOSAT-based inversions have a very pronounced seasonal cycle, but it does not match well with that derived from the surface-based stations.

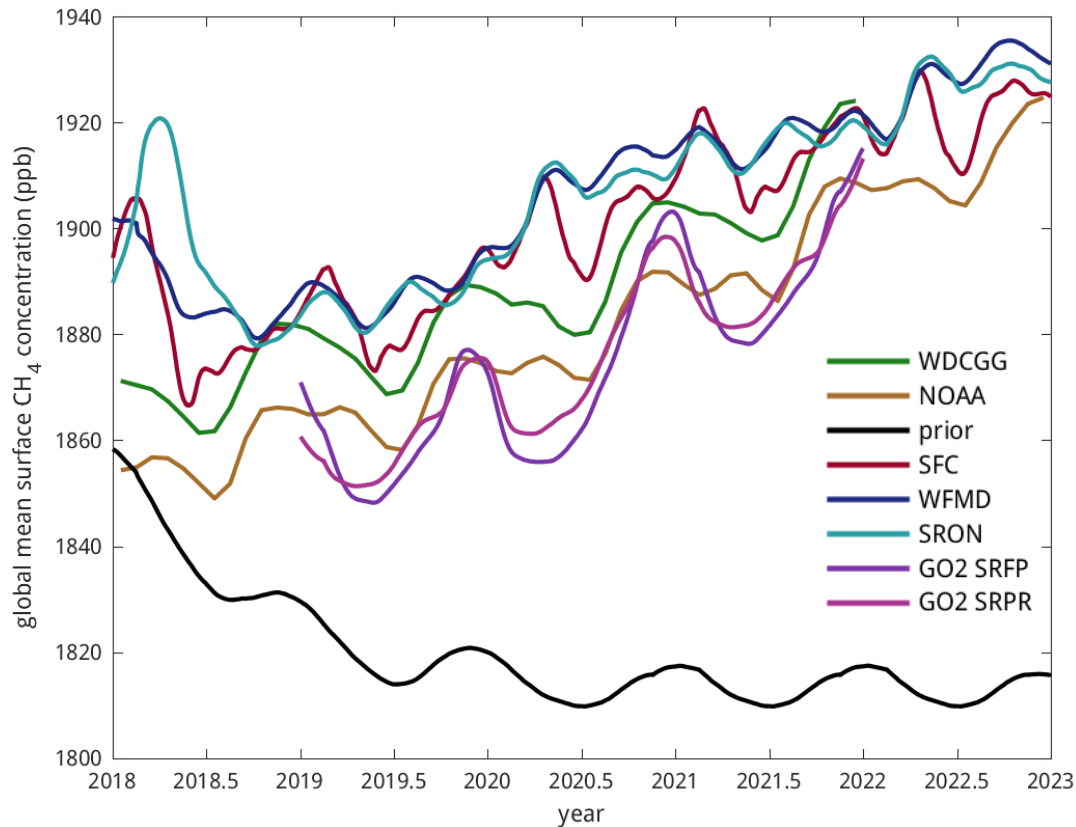|	ESA Climate Change Initiative (CCI+)	Page 27
ghg cci	**Climate Assessment Report (CAR)** for Climate Research Data Package 8 (CRDP#8)	Version 1.0
	of the Essential Climate Variable (ECV) Greenhouse Gases (GHG)	8 February 2024

Figure 9: Monthly global mean surface CH₄ mixing ratio at the surface, based directly on in situ measurements (for NOAA in brown and WDGCC in green) or from forward simulations of the prior (in black) or optimized fluxes, based on the surface network (red), CH4_S5P_WFMD (dark blue), CH4_S5P_SRON (light blue), CH4_GO2_SRFP (purple) and CH4_GO2_SRPR (magenta).

4.5.   Comparison of annual flux increments

To assess the spatial patterns inferred from the different inversions, the mean annual increment of the fluxes for 2020 is shown for each of the satellite inversions in Figure 10. The year 2020 was chosen for illustration in order to be able to compare all four satellite-based inversions side by side. Although the magnitudes shifted from year to year, the spatial pattern remained relatively constant.

What is encouraging: all inversions agree on the direction and location of the principal flux increments. These include the general decrease of the prior emissions over parts of China, as well as an increase in emissions in the Southern United States. A further robust pattern is a general increase in emissions from the Tropics. Specifically, all four inversions have larger increases in fluxes from eastern Africa, which is particularly pronounced for the two GOSAT-2-based inversions, as well as in Indonesia. The pattern over South America is more complex, with both positive and negative

anomalies found. Generally, there is a decrease in the prior emissions to the south and west, and a clear increase in emissions closer along the eastern coast of South America. The two TROPOMI-based inversions suggest that the prior emissions in Europe were too low, which is not found in the GOSAT-2-based inversions.
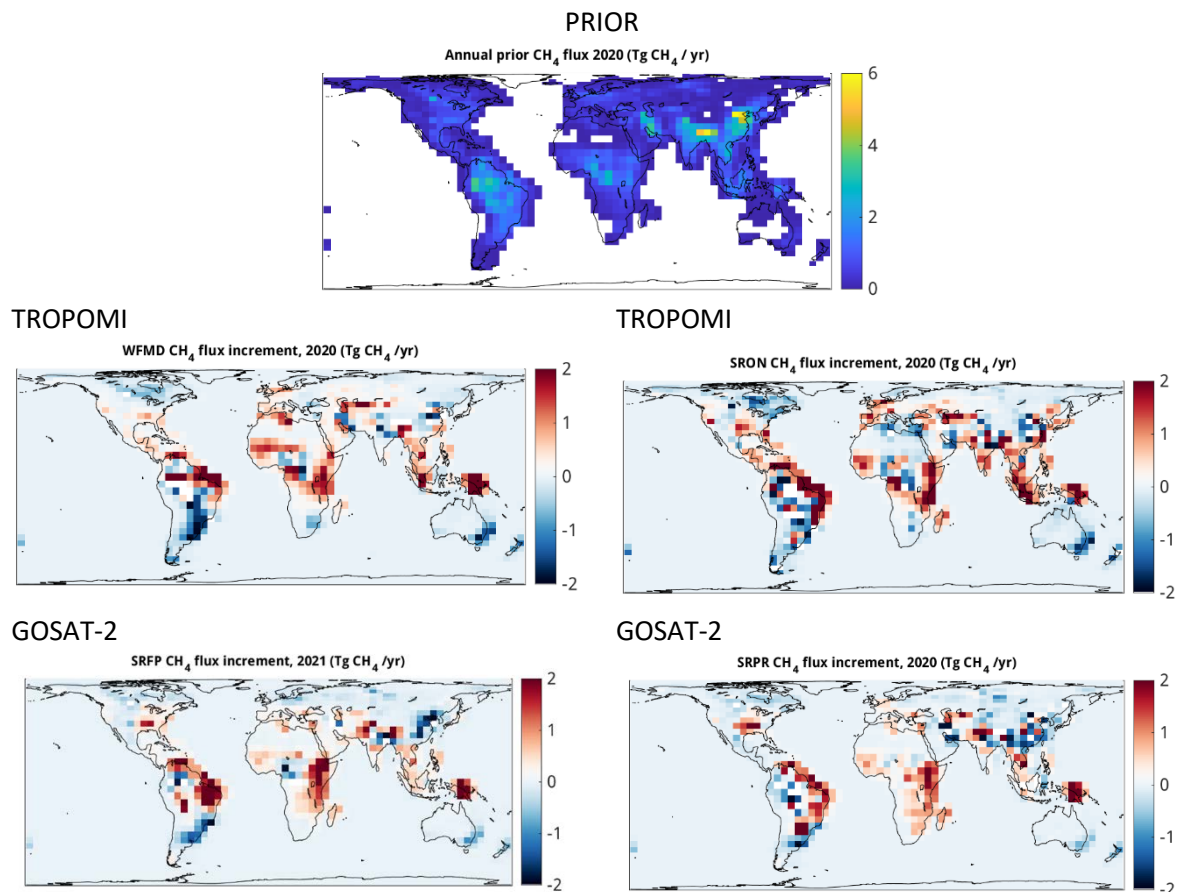

Figure 10: Annual flux increments for the four satellite-based inversions, along with the prior fluxes (at the top). The two TROPOMI inversions (CH4_S5P_WFMD, left, and CH4_S5P_SRON, right) are shown in the middle row, and the two GOSAT-2 inversions (CH4_GO2_SRFP, left, and CH4_GO2_SRPR, right) are shown in the bottom row.

Many of the patterns that are found in these flux increments are consistent with results from previous studies. Specifically:

- Basso et al. (2021) performed regional inversions over the Amazon region based on in situ aircraft-based profiles measurements, and found that the largest methane emissions were from the northeast coast of Brazil, as is seen in the anomaly maps in Figure 10.
- Several studies have shown that global bottom-up emission inventories (in this case, EDGAR 4.3.2) tend to overestimate anthropogenic methane emissions in China (e.g. Chen et al., 2022; Turner et al., 2015; the former based on TROPOMI data, the latter based on GOSAT data). The negative anomalies found in all the inversions confirm this finding.

	ESA Climate Change Initiative (CCI+)	Page 29
![ghg cci logo]	**Climate Assessment Report (CAR)** **for Climate Research Data Package 8 (CRDP#8)**	Version 1.0
	of the Essential Climate Variable (ECV) **Greenhouse Gases (GHG)**	8 February 2024

- The higher East African fluxes and reduced (but still substantial) West African fluxes are consistent with the findings of Lunt et al. (2019), which were based on inversions using GOSAT data.
- The flux anomalies found in North America, with increases in the Central Southern United States and decreases over much of Canada, are consistent with recent findings based on both in-situ and GOSAT-based inversions from Lu et al. (2022).

4.6.   Conclusions

The fluxes produced by assimilating both the WFMD and the SRON TROPOMI XCH$_4$ products into the Jena CarboScope show general structural agreement with each other, and result in similar near-surface concentrations as the fluxes resulting from the assimilation of surface-based measurements alone. This is in contrast to the GOSAT-2-based inversions, which result in a slightly low bias compared to the surface-based and TROPOMI-based inversions. The fact that the surface-based inversions and the TROPOMI-based inversions agree well with each other (see Figure 9) suggests that this is related to a low bias in the GOSAT-2 products.

Regardless, the pattern of flux increments is broadly similar when comparing the GOSAT-2-based and TROPOMI-based inversions, showing increases in fluxes in the Tropics, particularly in Indonesia, in Eastern Africa, and large positive anomalies along the northeastern coast in South America. These robust broad patterns are consistent across all the products considered, and are consistent with results from previous studies based on in situ and GOSAT (not GOSAT-2) measurements.

As in previous versions of the CAR, the resultant concentrations were compared to independent measurements using TCCON and (limited) aircraft-based measurements. As before, the satellite-based fluxes are better able to match the TCCON total column measurements, but the surface-based inversion does slightly better in reproducing independent aircraft measurements. This is also related to transport errors: the need for the bias correction (see Section 4.2) makes clear that the model cannot simultaneously match the surface measurements and the total column in a fully consistent way. Thus, this analysis is still not able to conclusively show a clear "winner" amongst the inversions. Furthermore, the global model is simply too coarse a tool to effectively make use of the high-resolution information that is provided by TROPOMI measurements, in particular. Indeed, to truly exploit the information content of the data, moving to much higher spatial resolutions than is possible with a global model is advised.

Despite this lack of conclusiveness, the better coverage of the CH4_S5P_WFMD retrieval, including more retrievals over the oceans, makes it the most attractive product for analysis. It also reports realistic measurement uncertainties, unlike the unrealistically low reported uncertainties of the SRON TROPOMI retrieval, which need to be inflated by the user to avoid overfitting. Though not officially part of the CDRP, a recommendation would be to make the reported uncertainties in the CH4_S5P_SRON more realistic, making it easier for users to properly interpret. A concrete, if minor,

recommendation for the retrieval team for the GOSAT-2 product is to include orbit numbers in the data files.

Despite the general agreement that is seen in concentration space, the temporal and spatial variability of the fluxes that arise from the assimilation of TROPOMI XCH_4 are still quite variable in both space and time, leading to unrealistically large seasonal cycles, particularly for boreal regions. The experimental setup exacerbates this problem: because the XCH_4 products were assimilated alone, there was no stabilizing influence from simultaneously assimilated surface measurements. Because the spatial coverage of the measurements has such a strong seasonal cycle, small systematic errors, especially at high latitudes, can induce unrealistic fluxes. Here the recommendation is rather on the user side: simultaneously assimilating surface-based and satellite data can mitigate these effects.

Despite these concerns, the amount of detailed information about local methane gradients in the TROPOMI retrieval products is extraordinary, and the products have already been used extensively to analyze point sources and local-scale gradients. They are also able to well reproduce global mean mixing ratios over the five years considered in this report. Nonetheless, for their application in global inversion modelling to analyse regional scale fluxes over seasonal and interannual scales, care needs to be taken to ensure that (perhaps small) systematic errors do not bias the resultant fluxes. Compared to the results from CAR7, the GOSAT-2 retrievals appear to be significantly improved in terms of noisiness, potentially as a result of the improved data screening, but the results suggest a low bias.

	ESA Climate Change Initiative (CCI+)	Page 31
ghg cci	**Climate Assessment Report (CAR)** for Climate Research Data Package 8 (CRDP#8)	Version 1.0
	of the Essential Climate Variable (ECV) Greenhouse Gases (GHG)	8 February 2024

Acknowledgements

	ESA Climate Change Initiative (CCI+)	Page 32
ghg cci	**Climate Assessment Report (CAR)** for Climate Research Data Package 8 (CRDP#8)	Version 1.0
	of the Essential Climate Variable (ECV) Greenhouse Gases (GHG)	8 February 2024

References

Note:

- *Links to pdf versions of all GHG-CCI+ CRDP documents are available on the GHG-CCI+ key documents website: https://climate.esa.int/en/projects/ghgs/key-documents/*
- *Links to pdf versions of all GHG-CCI+ publications are available on the GHG-CCI+ publications website: https://climate.esa.int/en/projects/ghgs/publications/*

Alexe, M., P. Bergamaschi, A. Segers, et al., Inverse modeling of CH_4 emissions for 2010–2011 using different satellite retrieval products from GOSAT and SCIAMACHY, *Atmos. Chem. Phys.*, 15, 113–133, doi:10.5194/acp-15-113-2015, 2015.

Balasus, N., Jacob, D. J., Lorente, A., Maasakkers, J. D., Parker, R. J., Boesch, H., Chen, Z., Kelp, M. M., Nesser, H., and Varon, D. J.: A blended TROPOMI+GOSAT satellite data product for atmospheric methane using machine learning to correct retrieval biases, Atmos. Meas. Tech., 16, 3787–3807, https://doi.org/10.5194/amt-16-3787-2023, 2023.

Basso, L.S., Marani, L., Gatti, L.V. et al. Amazon methane budget derived from multi-year airborne observations highlights regional variations in emissions. Commun Earth Environ 2, 246, https://doi.org/10.1038/s43247-021-00314-4, 2021.

Bastos, A., Running, S.W., Gouveia, C. and Trigo, R.M: The global NPP dependence on ENSO: La-Nina and the extraordinary year of 2011. *J. Geophys. Res*. 118, 1247–1255, 2013

Basu, S., Guerlet, S., Butz, A., et al., Global CO_2 fluxes estimated from GOSAT retrievals of total column CO_2, *Atmos. Chem. Phys.*, 13, 8695-8717, 2013.

Basu, S., Krol, M., Butz, A., et al., The seasonal variation of the CO_2 flux over Tropical Asia estimated from GOSAT, CONTRAIL and IAS, *Geophys. Res. Lett.*, doi: 10.1002/2013GL059105, 2014.

Bergamaschi, P., C. Frankenberg, J. F. Meirink, M. Krol, M. G. Villani, S. Houweling, F. Dentener, E. J. Dlugokencky, J. B. Miller, L. V. Gatti, A. Engel, and I. Levin: Inverse modeling of global and regional CH_4 emissions using SCIAMACHY satellite retrievals, *J. Geophys. Res.*, 114, doi:10.1029/2009JD012287, 2009.

Bergamaschi, P., et al.: Inverse modeling of European CH_4 emissions 2001-2006, *J. Geophys. Res*., 115(D22309), doi:10.1029/2010JD014180, 2010.

Bergamaschi, P., S. Houweling, A. Segers, M. Krol, C. Frankenberg, R. A. Scheepmaker, E. Dlugokencky, S. Wofsy, E. Kort, C. Sweeney, T. Schuck, C. Brenninkmeijer, H. Chen, V. Beck and C. Gerbig, Atmospheric CH_4 in the first decade of the 21st century: Inverse modeling analysis using SCIAMACHY satellite retrievals and NOAA surface measurements, *J. Geophys. Res.*, 118, doi:10.1002/jgrd.50480, 2013.

Bloom, A. A., Palmer, P. I., Fraser, A., and Reay, D. S.: Seasonal variability of tropical wetland CH4 emissions: the role of the methanogen-available carbon pool, *Biogeosciences*, 9, 2821–2830, doi:10.5194/bg-9-2821-2012, 2012

Boden, T. A., Marland, G., and Andres, R. J.: Global, regional, and national fossil-fuel CO2 emissions. Carbon Dioxide Information Analysis Center, Oak Ridge National Laboratory, U.S. Department of Energy, Oak Ridge, Tenn., U.S.A., Doi:10.3334/CDIAC/00001_V2013, 2013

Buchwitz, M., M. Reuter, O. Schneising, et al., The Greenhouse Gas Climate Change Initiative (GHG-CCI): comparison and quality assessment of near-surface-sensitive satellite-derived CO_2 and CH_4 global data sets, *Remote Sensing of Environment*, 162, 344–362, doi:10.1016/j.rse.2013.04.024, 2015.

Buchwitz, M., M. Reuter, O. Schneising, W. Hewson, R.G. Detmers, H. Boesch, O.P. Hasekamp, I. Aben, H. Bovensmann, J.P. Burrows, A. Butz, F. Chevallier, B. Dils, C. Frankenberg, J. Heymann, G. Lichtenberg, M. De Mazière, J. Notholt, R. Parker, T. Warneke, C. Zehner, D.W.T. Griffith, N.M. Deutscher, A. Kuze, H. Suto, D. Wunch, 2017: Global satellite observations of column-averaged carbon dioxide and methane: The GHG-CCI XCO_2 and XCH_4 CRDP3 data set, Remote Sensing of Environment, 203, 276-295, doi:dx.doi.org/10.1016/j.rse.2016.12.027.

Buchwitz, M., Dils, B., Reuter, M., Schneising, O., Hilker, M., Preval, S., Boesch, H., Borsdoff, T., Landgraf, J., Krisna, T.C., Product Validation and Intercomparison Report (PVIR) for the Essential Climate Variable (ECV) Greenhouse Gases (GHG): XCO_2 and/or XCH_4 from OCO-2, TanSat, Sentinel-5-Precursor and GOSAT-2, v3.0, 16 February 2022, 2022.

Butz, A., Guerlet, S., Hasekamp, O., et al., Toward accurate CO_2 and CH_4 observations from GOSAT, *Geophys. Res. Lett.*, doi:10.1029/2011GL047888, 2011.

Byrne, B., Baker, D. F., Basu, S., et al.: National CO_2 budgets (2015–2020) inferred from atmospheric CO2 observations in support of the global stocktake, Earth Syst. Sci. Data, 15, 963–1004, https://doi.org/10.5194/essd-15-963-2023, 2023.

Canadell, J. G., Ciais, P., Dhakal, S., et al., Interactions of the carbon cycle, human activity, and the climate system: a research portfolio, *Curr. Opin. Environ. Sustainabil.*, 2, 301–311, 2010.

Chatterjee, A., Gierach, M. M., Sutton, A. J. et al., Influence of El Niño on atmospheric CO_2 over the tropical Pacific Ocean: Findings from NASA's OCO-2 mission. Science 358, eaam5776, doi:10.1126/science.aam5776, 2017.

Chen, Z., Jacob, D. J., Nesser, H., Sulprizio, M. P., Lorente, A., Varon, D. J., Lu, X., Shen, L., Qu, Z., Penn, E., and Yu, X.: Methane emissions from China: a high-resolution inversion of TROPOMI satellite observations, Atmos. Chem. Phys., 22, 10809–10826, https://doi.org/10.5194/acp-22-10809-2022, 2022.

Chevallier, F., et al.: Inferring CO_2 sources and sinks from satellite observations: method and application to TOVS data. *J. Geophys. Res*., 110, D24309, 2005.

Chevallier, F.: Impact of correlated observation errors on inverted CO2 surface fluxes from OCO measurements, *Geophys. Res. Lett.*, 34, L24804, doi:10.1029/2007GL030463, 2007.

Chevallier, F., Maksyutov, S., Bousquet, P., Bréon, F.-M., Saito, R., Yoshida, Y., and Yokota, T.: On the accuracy of the CO_2 surface fluxes to be estimated from the GOSAT observations. *Geophys. Res. Lett*., 36, L19807, doi:10.1029/2009GL040108, 2009.

Chevallier, F., et al.: CO_2 surface fluxes at grid point scale estimated from a global 21-year reanalysis of atmospheric measurements. *J. Geophys. Res*., 115, D21307, doi:10.1029/2010JD013887, 2010a.

Chevallier, F., Feng, L., Boesch, H., Palmer, P., and Rayner, P.: On the impact of transport model errors for the estimation of CO_2 surface fluxes from GOSAT observations. *Geophys. Res. Lett*., 37, L21803, doi:10.1029/2010GL044652, 2010b.

Chevallier, F., Deutscher, N. M., Conway, T. J., Ciais, P., Ciattaglia, L., Dohe, S., Frohlich, M., Gomez-Pelaez, A. J., Griffith, D., Hase, F., Haszpra, L., Krummel, P., Kyro, E., Labuschagne, C., Langenfelds, R., Machida, T., Maignan, F., Matsueda, H., Morino, I., Notholt, J., Ramonet, M., Sawa, Y., Schmidt, M., Sherlock, V., Steele, P., Strong, K., Sussmann, R., Wennberg, P., Wofsy, S., Worthy, D., Wunch, D., and Zimnoch, M.: Global CO_2 fluxes inferred from surface air-sample measurements and from TCCON retrievals of the CO_2 total column, *Geophys. Res. Lett*., 38, L24810, doi:10.1029/2011GL049899, 2011

Chevallier, F., Bergamaschi, P., Kaminiski, T., Scholze, M., Climate Assessment Report (CAR) for the GHG-CCI project of ESA's Climate Change Initiative, version 1.1 (CARv1.1), 18. Nov. 2013, 2013.

Chevallier, F., and O'Dell, C. W., Error statistics of Bayesian CO_2 flux inversion schemes as seen from GOSAT, *Geophys. Res. Lett.*, doi: 10.1002/grl.50228, 2013.

Chevallier, F., Palmer, P.I., Feng, L., Boesch, H., O'Dell, C.W., Bousquet, P., Towards robust and consistent regional CO_2 flux estimates from in situ and space-borne measurements of atmospheric CO_2, *Geophys. Res. Lett.*, 41, 1065-1070, DOI: 10.1002/2013GL058772, 2014a.

Chevallier, F., Buchwitz, M., Bergamaschi, et al., User Requirements Document for the GHG-CCI project of ESA's Climate Change Initiative, version 2 (URDv2), 28. August 2014, 2014b.

Chevallier, F.: On the statistical optimality of CO_2 atmospheric inversions assimilating CO_2 column retrievals, Atmos. Chem. Phys., 15, 11133–11145, https://doi.org/10.5194/acp-15-11133-2015, 2015.

Chevallier, F., P. Bergamaschi, D. Brunner, S. Gonzi, S. Houweling, T. Kaminski, G. Kuhlmann, T. T. van Leeuwen, J. Marshall, P. I. Palmer, and M. Scholze, Climate Assessment Report for the GHG-CCI project of ESA's Climate Change Initiative, pp. 87, version 2, 22 April 2015, 2015.

Chevallier, F., M. Alexe, P. Bergamaschi, D. Brunner, L. Feng, S. Houweling, T. Kaminski, W. Knorr, T. T. van Leeuwen, J. Marshall, P. I. Palmer, M. Scholze, A.-M. Sundström and M. Voßbeck, Climate Assessment Report for the GHG-CCI project of ESA's Climate Change Initiative, pp. 94, version 3, 3 May 2016, 2016.

Chevallier, F., P. Bergamaschi, D. Brunner, L. Feng, S. Houweling, T. Kaminski, W. Knorr, J. Marshall, P. I. Palmer, S. Pandey, M. Reuter, M. Scholze, and M. Voßbeck, Climate Assessment Report for the GHG-CCI project of ESA's Climate Change Initiative, pp. 96, version 4,, 27 March 2017, 2017.

Chevallier, F., Remaud, M., O'Dell, C. W., Baker, D., Peylin, P., and Cozic, A.: Objective evaluation of surface- and satellite-driven carbon dioxide atmospheric inversions, Atmos. Chem. Phys., 19, 14233–14251, https://doi.org/10.5194/acp-19-14233-2019, 2019.

Chevallier, F., Climate Assessment Report for the GHG-CCI+ project of ESA's Climate Change Initiative, pp. 36, version 1.2, 20 March 2020, 2020.

Chevallier, F. and Marshall, J., Climate Assessment Report for the GHG-CCI+ project of ESA's Climate Change Initiative, pp. 59, version 2.0, 9 March 2021, 2021.

Chevallier, F., Evaluation and Quality Control document for observation-based CO_2 flux estimates for the period 1979 – 2022, v21r2. CAMS deliverable CAMS255_2021SC1_D55.1.4.2-2023_202308. http://atmosphere.copernicus.eu/, 2023a.

Chevallier, F., Evaluation and Quality control document for the analyses of the OCO-2 record [satellite-driven CO2 inversion FT23r1]. CAMS deliverable CAMS255_2021SC1_D1.4.1-2023-2_202308. http://atmosphere.copernicus.eu/, 2023b.

Chevallier, F. and Marshall, J., Climate Assessment Report for Climate Research Data Package No. 7 (CRDP#7) of ESA's Climate Change Initiative project GHG-CCI+, version 1.1, 20 March 2023, 2023.

Chevallier, F., Lloret, Z., Cozic, A., Takache, S., & Remaud, M. (2023). Toward high-resolution global atmospheric inverse modelling using graphics accelerators. Geophysical Research Letters, 50, e2022GL102135. https://doi.org/10.1029/2022GL102135

Cogan, A. J., Boesch, H., Parker, R. J., et al., Atmospheric carbon dioxide retrieved from the Greenhouse gases Observing SATellite (GOSAT): Comparison with ground-based TCCON observations and GEOS-Chem model calculations, *J. Geophys. Res.*, 117, D21301, doi:10.1029/2012JD018087, 2012.

Conway, T. J., Tans, P. P., Waterman, L. S., Thoning, K. W., Kitzis, D. R., Masarie, K. A. and Zhang, N.: Evidence for interannual variability of the carbon cycle from the National Oceanic and Atmospheric Administration/Climate Monitoring and Diagnostics Laboratory Global Air Sampling Network, *J. Geophys. Res.*, 99(D11), 22,831–22,855, doi:10.1029/94JD01951, 1994

Cramer, W., Kicklighter, D. W., Bondeau, A., Iii, B. M., Churkina, G., Nemry, B., Ruimy, A., Schloss, A. L. and Intercomparison, ThE. P. OF. ThE. P. NpP. M., Comparing global models of terrestrial net primary

productivity (NPP): overview and key results. *Global Change Biology*, 5: 1–15. doi:10.1046/j.1365-2486.1999.00009.x, 1999.

Cressot, C., F. Chevallier, P. Bousquet, et al., On the consistency between global and regional methane emissions inferred from SCIAMACHY, TANSO-FTS, IASI and surface measurements, *Atmos. Chem. Phys.*, 14, 577-592, 2014.

Cressot, C., Pison, I., Rayner, P. J., Bousquet, P., Fortems-Cheiney, A., and Chevallier, F.: Can we detect regional methane anomalies? A comparison between three observing systems, Atmos. Chem. Phys., 16, 9089-9108, doi:10.5194/acp-16-9089-2016, 2016.

Crevoisier, C., Sweeney, C., Gloor, M., Sarmiento, J. L., and Tans, P. P.: Regional U.S. carbon sinks from three-dimensional atmospheric CO_2 sampling, *Proc. Natl. Acad. Sci.* (2010), 107: 18348-18353, 2010.

Crowell, S., Baker, D., Schuh, A., Basu, S., Jacobson, A. R., Chevallier, F., Liu, J., Deng, F., Feng, L., McKain, K., Chatterjee, A., Miller, J. B., Stephens, B. B., Eldering, A., Crisp, D., Schimel, D., Nassar, R., O'Dell, C. W., Oda, T., Sweeney, C., Palmer, P. I., and Jones, D. B. A.: The 2015–2016 carbon cycle as seen from OCO-2 and the global in situ network, Atmos. Chem. Phys., 19, 9797–9831, https://doi.org/10.5194/acp-19-9797-2019, 2019.

Dee, D. P., et al., The ERA-Interim reanalysis: configuration and performance of the data assimilation system, Q. J. R. Meteorol. Soc., 137, 553–597, 2011.

Desroziers G., Berre, L., Chapnik, B., and Poli, P.: Diagnosis of observation, background and analysis error statistics in observation space. *Q. J. Roy. Meteor. Soc.*, 131, 3385-3396, 2005.

Detmers, R., Hasekamp, O., Aben, I., Houweling, S., van Leeuwen, T.T., Butz, A., Landgraf, J., Kohler, P., Guanter, L., and Poulter, B.: Anomalous carbon uptake in Australia as seen by GOSAT. *Geophysical Research Letters*, 42(19), 2015

Dlugokencky, E. J., L. P. Steele, P. M. Lang, and K. A. Masarie, The growth rate and distribution of atmospheric methane, *J. Geophys. Res.*, 99, 17021–17043. 1994.

Dlugokencky, E. J., S. Houweling, L. Bruhwiler, K. A. Masarie, P.M. Lang, J. B. Miller, and P. P. Tans, Atmospheric methane levels off: Temporary pause or a new steady-state? *Geophys. Res. Lett.*, 30(19), 1992, doi:10.1029/2003GL018126, 2003.

Dlugokencky, E. J., Bruhwiler, L., White, J. W. C., et al., Observational constraints on recent increases in the atmospheric CH_4 burden, *Geophys. Res. Lett.*, 36, L18803, doi:10.1029/2009GL039780, 2009.

Dlugokencky, E., P. Lang, J. Mund, A. Crotwell, M. Crotwell, and K. Thoning, Atmospheric carbon dioxide dry air mole fractions from the NOAA ESRL carbon cycle cooperative global air sampling network, 1968-2015, 2016.

Dubovik, O. and King, M. D.: A flexible inversion algorithm for retrieval of aerosol optical properties from Sun and sky radiance measurements, *J. Geophys. Res*., 105, 20673–20696, 2000.

Enting, I. G.: Inverse Problems in Atmospheric Constituent Transport. Cambridge University Press, 2002.

ESA: A-SCOPE - Advanced Space Carbon and Climate Observation of Planet Earth, Technical Report SP-1313/1, European Space Agency, Noordwijk, The Netherlands. 2008

Feng, L., Palmer, P. I., Bösch, H., and Dance, S.: Estimating surface CO_2 fluxes from space-borne CO_2 dry air mole fraction observations using an ensemble Kalman Filter, *Atmos. Chem. Phys*., 9, 2619–2633, doi:10.5194/acp-9-2619-2009, 2009.

Feng, L., P. I. Palmer, R. J. Parker, et al., Estimates of European uptake of CO_2 inferred from GOSAT X_{CO2} retrievals: sensitivity to measurement bias inside and outside Europe, *Atmos. Chem. Phys*., 16, 1289-1302, doi:10.5194/acp-16-1289-2016, 2016a.

Feng, L., Palmer, P. I., Bösch, H., Parker, R. J., Webb, A. J., Correia, C. S. C., Deutscher, N. M., Domingues, L. G., Feist, D. G., Gatti, L. V., Gloor, E., Hase, F., Kivi, R., Liu, Y., Miller, J. B., Morino, I., Sussmann, R., Strong, K., Uchino, O., Wang, J., and Zahn, A.: Consistent regional fluxes of CH4 and CO2 inferred from GOSAT proxy XCH4:XCO2 retrievals, 2010–2014, Atmos. Chem. Phys. Discuss., doi:10.5194/acp-2016-868, in review, 2016b.Frankenberg, C., Aben, I., Bergamaschi, P., et al., Global column-averaged methane mixing ratios from 2003 to 2009 as derived from SCIAMACHY: Trends and variability, *J. Geophys. Res*., doi:10.1029/2010JD014849, 2011.

Feng, L., Palmer, P.I., Zhu, S. et al. Tropical methane emissions explain large fraction of recent changes in global atmospheric methane growth rate. Nat Commun 13, 1378, https://doi.org/10.1038/s41467-022-28989-z, 2022.

Frankenberg, C, Product User Guide (PUG) for the IMAP-DOAS XCH4 SCIAMACHY Data Products, version 1, ESA Climate Change Initiative (CCI) GHG-CCI project, 13 Dec. 2012, 2012.

Fraser, A., Palmer, P. I., Feng, L., et al., Estimating regional methane surface fluxes: the relative importance of surface and GOSAT mole fraction measurements, *Atmos. Chem. Phys*., 13, 5697-5713, doi:10.5194/acp-13-5697-2013, 2013.

Fraser, A., Palmer, P. I., Feng, L. et al., Estimating regional fluxes of CO_2 and CH_4 using space-borne observations of $XCH_4:XCO_2$, *Atmos. Chem. Phys.*, 14, 12883-12895, doi:10.5194/acp-14-12883-2014, 2014.

Friedl, M. A., Strahler, A. H., and Hodges, J.: ISLSCP II MODIS (Collection 4) IGBP Land Cover, 2000–2001, in: ISLSCP Initia- tive II Collection, Data set, edited by: Hall, F. G., Collatz, G., Meeson, B., Los, S., Brown de Colstoun, E., and Landis, D., Oak Ridge National Laboratory Distributed Active Archive Center, Oak Ridge, Tennessee, USA, doi:10.3334/ORNLDAAC/96

Friedlingstein, P., O'Sullivan, M., Jones, M. W., Andrew, R. M., Gregor, L., Hauck, J., Le Quéré, C., Luijkx, I. T., Olsen, A., Peters, G. P., Peters, W., Pongratz, J., Schwingshackl, C., Sitch, S., Canadell, J. G., Ciais, P., Jackson, R. B., Alin, S. R., Alkama, R., Arneth, A., Arora, V. K., Bates, N. R., Becker, M., Bellouin, N., Bittig, H. C., Bopp, L., Chevallier, F., Chini, L. P., Cronin, M., Evans, W., Falk, S., Feely, R. A., Gasser, T., Gehlen, M., Gkritzalis, T., Gloege, L., Grassi, G., Gruber, N., Gürses, Ö., Harris, I., Hefner, M., Houghton, R. A., Hurtt, G. C., Iida, Y., Ilyina, T., Jain, A. K., Jersild, A., Kadono, K., Kato, E., Kennedy, D., Klein Goldewijk, K., Knauer, J., Korsbakken, J. I., Landschützer, P., Lefèvre, N., Lindsay, K., Liu, J., Liu, Z., Marland, G., Mayot, N., McGrath, M. J., Metzl, N., Monacci, N. M., Munro, D. R., Nakaoka, S.-I., Niwa, Y., O'Brien, K., Ono, T., Palmer, P. I., Pan, N., Pierrot, D., Pocock, K., Poulter, B., Resplandy, L., Robertson, E., Rödenbeck, C., Rodriguez, C., Rosan, T. M., Schwinger, J., Séférian, R., Shutler, J. D., Skjelvan, I., Steinhoff, T., Sun, Q., Sutton, A. J., Sweeney, C., Takao, S., Tanhua, T., Tans, P. P., Tian, X., Tian, H., Tilbrook, B., Tsujino, H., Tubiello, F., van der Werf, G. R., Walker, A. P., Wanninkhof, R., Whitehead, C., Willstrand Wranne, A., Wright, R., Yuan, W., Yue, C., Yue, X., Zaehle, S., Zeng, J., and Zheng, B.: Global Carbon Budget 2022, Earth Syst. Sci. Data, 14, 4811–4900, https://doi.org/10.5194/essd-14-4811-2022, 2022.

Fuentes Andrade, B., Buchwitz, M., Reuter, M., Bovensmann, H., Richter, A., Boesch, H., and Burrows, J. P.: A method for estimating localized CO_2 emissions from co-located satellite XCO_2 and NO_2 images, EGUsphere [preprint], https://doi.org/10.5194/egusphere-2023-2085, 2023.

Gatti, L. V., Gloor, M., Miller, J. B., Doughty, C. E., Malhi, Y., Domingues, L. G., Basso, L. S., Martinewski, A., Correia, C. S. C., Borges, V. F., Freitas, S., Braz, R., Anderson, L. O., Rocha, H., Grace, J., Philips, O. L., and Lloyd, J.: Drought sensitivity of Amazonian carbon balance revealed by atmospheric measurements, *Nature*, 506(7486), 76-80, doi:10.1038/nature12957, 2014

Gao, M., Xing, Z., Vollrath, C. et al. Global observational coverage of onshore oil and gas methane sources with TROPOMI. Sci Rep 13, 16759, https://doi.org/10.1038/s41598-023-41914-8, 2023.

Cooperative Global Atmospheric Data Integration Project. (2020). *Multi-laboratory compilation of atmospheric carbon dioxide data for the period 1957-2019; obspack_co2_1_GLOBALVIEWplus_v6.0_2020_09_11* [Data set]. NOAA Earth System Research Laboratory, Global Monitoring Division. https://doi.org/10.25925/20200903

Guerlet, S., Basu, S., Butz, A., et al., Reduced carbon uptake during the 2010 Northern Hemisphere summer from GOSAT, *Geophys. Res. Lett.*, doi: 10.1002/grl.50402, 2013.

Gurney, K.R., et al.: Towards robust regional estimates of CO_2 sources and sinks using atmospheric transport models. *Nature*, 415:6872, 626-630, 2002.

Harris, I., Jones, P.D., Osborn, T.J. and Lister, D.H., Updated high-resolution grids of monthly climatic observations – the CRU TS3.10 Dataset. *Int. J. Climatol*. doi: 10.1002/joc.3711, 2013

Haverd, V., Raupach, M. R., Briggs, P. R., J. G. Canadell., Davis, S. J., Law, R. M., Meyer, C. P., Peters, G. P., Pickett-Heaps, C., and Sherman, B.: The Australian terrestrial carbon budget, *Biogeosciences*, 10, 851-869, doi:10.5194/bg-10-851-2013, 2013.

Hayman, G. D., O'Connor, F. M., Dalvi, et al., Comparison of the HadGEM2 climate-chemistry model against in-situ and SCIAMACHY atmospheric methane data, *Atmos. Chem. Phys.*, 14, 13257-13280, doi:10.5194/acp-14-13257-2014, 2014.

Heimann, M.: The global atmospheric tracer model TM2, Technical Report No. 10, Max-Planck-Institut für Meteorologie, Hamburg, Germany. 1995

Heimann, M., G. Esser, A. Haxeltine, J. Kaduk, D.W. Kicklighter, W. Knorr, G. H. Kohlmaier, A. D. McGuire, J. Melillo, B. Moore, et al., Evaluation of terrestrial carbon cycle models through simulations of the seasonal cycle of atmospheric CO2: First results of a model intercomparison study, Global Biogeochemical Cycles, 12, 1–24, 1998.

Heimann, M. and S. Körner: The global atmospheric tracer model TM3. In: Max-Planck-Institut für Biogeochemie (Eds.): Technical Report. Vol. 5. Max-Planck-Institut für Biogeochemie, Jena. pp. 131, 2003.

Heymann, J., Schneising, O., Reuter, M., et al., SCIAMACHY WFM-DOAS XCO_2: comparison with CarbonTracker XCO_2 focusing on aerosols and thin clouds, *Atmos. Meas. Tech.*, 5, 1935-1952, 2012.

Hourdin, F., Rio, C., Grandpeix, J.-Y., Madeleine, J.-B., Cheruy, F., Rochetin, N., et al. (2020). LMDZ6A: The atmospheric component of the IPSL climate model with improved and better tuned physics. *Journal of Advances in Modeling Earth Systems*, 12(7), e2019MS001892. https://doi.org/10.1029/2019MS001892

Houweling, S., et al.: The importance of transport model uncertainties for the estimation of CO_2 sources and sinks using satellite measurements. *Atmos. Chem. Phys.*, 10, 9981-9992, doi:10.5194/acp-10-9981-2010, 2010.

Houweling, S., M. Krol, P. Bergamaschi, C. Frankenberg, E. J. Dlugokencky, I. Morino, J. Notholt, V. Sherlock, D. Wunch, V. Beck, C. Gerbig, H. Chen, E. A. Kort, T. Röckmann and I. Aben, A multi-year methane inversion using SCIAMACHY, accounting for systematic errors using TCCON measurements, *Atmos. Chem. Phys.*, 14, 3991–4012, doi:10.5194/acp-14-3991-2014, 2014.

Houweling, S., D. Baker, S. Basu, H. Boesch, A. Butz, F. Chevallier, F. Deng, E. Dlugockencky, L. Feng, A. Ganshin, O. P. Hasekamp, D. Jones, S. Maksyutov, J. Marshall, T. Oda, C. O'Dell, S. Oshchepkov, P. Paul, P. Peylin, Z. Poussi, F. Reum, H. Takagi, Y. Yoshida, R. Zhuravlev, An inter-comparison of inverse models for estimating sources and sinks of CO_2 using GOSAT measurements. *J. Geophys. Res. Atmos.*, 120, 5253–5266, doi:10.1002/2014JD022962, 2015.

	ESA Climate Change Initiative (CCI+)	Page 40
ghg cci	**Climate Assessment Report (CAR)** for Climate Research Data Package 8 (CRDP#8)	Version 1.0
	of the Essential Climate Variable (ECV) Greenhouse Gases (GHG)	8 February 2024

Hu, H., Hasekamp, O., Butz, A., Galli, A., Landgraf, J., Aan de Brugh, J., Borsdorff, T., Scheepmaker, R., and Aben, I.: The operational methane retrieval algorithm for TROPOMI, Atmos. Meas. Tech., 9, 5423–5440, https://doi.org/10.5194/amt-9-5423-2016, 2016.

Kirschke, S., Bousquet, P., Ciais, P., et al., Three decades of global methane sources and sinks, *Nat. Geosci.*, 6, 813–823, doi:10.1038/ngeo1955, 2013.

Kort, E. A., Frankenberg, C., Costigan, K. R., et al., Four corners: The largest US methane anomaly viewed from space, *Geophys. Res. Lett.*, 41, doi:10.1002/2014GL061503, 2014.

Krisna, T. C., et al.: ESA Climate Change Initiative "Plus" (CCI+) Product User Guide (PUG) Version 3.0 for the RemoTeC XCO2 GOSAT-2 SRON Full-Physics Product (CO2_GO2_SRFP) Version 2.0.0, Technical Report, pp. 21, https://www.iup.uni-bremen.de/carbon_ghg/docs/GHG-CCIplus/CRDP7/PUGv3_GHG-CCI_CO2_GO2_SRFP_v2.0.0.pdf, 2022a.

Krisna, T. C., et al.: ESA Climate Change Initiative "Plus" (CCI+) Product User Guide (PUG) Version 3.0 for the RemoTeC XCH4 GOSAT-2 PROXY Product (CH4_GO2_SRPR) version 2.0.0, https://www.iup.uni-bremen.de/carbon_ghg/docs/GHG-CCIplus/CRDP7/PUGv3_GHG-CCI_CH4_GO2_SRPR_v2.0.0.pdf, 2022b.

Krol, M. C., S. Houweling, B. Bregman, M. van den Broek, A. Segers, P. van Velthoven, W. Peters, F. Dentener, and P. Bergamaschi, The two-way nested global chemistry-transport zoom model TM5: algorithm and applications, *Atmos. Chem. Phys.*, 5, 417-432, 2005.

Lan, X., K.W. Thoning, and E.J. Dlugokencky: Trends in globally-averaged CH_4, N_2O, and SF_6 determined from NOAA Global Monitoring Laboratory measurements. Version 2023-01, https://doi.org/10.15138/P8XG-AA10, 2022.

Lauvaux, T., Giron, C., Mazzolini, M. et al., Global assessment of oil and gas methane ultra-emitters. Science 375, 557-561 doi:10.1126/science.abj4351, 2022.

Liang, R., Zhang, Y., Chen, W., Zhang, P., Liu, J., Chen, C., Mao, H., Shen, G., Qu, Z., Chen, Z., Zhou, M., Wang, P., Parker, R. J., Boesch, H., Lorente, A., Maasakkers, J. D., and Aben, I.: East Asian methane emissions inferred from high-resolution inversions of GOSAT and TROPOMI observations: a comparative and evaluative analysis, Atmos. Chem. Phys., 23, 8039–8057, https://doi.org/10.5194/acp-23-8039-2023, 2023.

Lindqvist, H., C. W. O'Dell, S. Basu, H. Boesch, F. Chevallier, N. Deutscher, L. Feng, B. Fisher, F. Hase, M. Inoue, R. Kivi, I. Morino, P. I. Palmer, R. Parker, M. Schneider, R. Sussmann, and Y. Yoshida, Does GOSAT capture the true seasonal cycle of carbon dioxide?; *Atmos. Chem. Phys.*, 15, 13023-13040, doi:10.5194/acp-15-13023-2015, 2015.

Liu, J., K. W. Bowman, D. Schimel, N. C. Parazoo, Z. Jiang, M. Lee, A. A. Bloom, D. Wunch, C. Frankenberg, Y.Sun, C. W. O'Dell, K. R. Gurney, D. Menemenlis, M. Girerach, D. Crisp, and A. Eldering,

	ESA Climate Change Initiative (CCI+)	Page 41
ghg cci	**Climate Assessment Report (CAR)** for Climate Research Data Package 8 (CRDP#8)	Version 1.0
	of the Essential Climate Variable (ECV) Greenhouse Gases (GHG)	8 February 2024

Contrasting carbon cycle responses of the tropical continents to the 2015–2016 El Niño. Science 358, doi:10.1126/science.aam5690, 2017.

R. Gurney, D. Menemenlis, M. Girerach, D. Crisp, and A. Eldering, Contrasting carbon cycle responses of the tropical continents to the

2015–2016 El Niño. Science 358, eaam5690 (2017Lorente, A., Borsdorff, T., Butz, A., Hasekamp, O., aan de Brugh, J., Schneider, A., Wu, L., Hase, F., Kivi, R., Wunch, D., Pollard, D. F., Shiomi, K., Deutscher, N. M., Velazco, V. A., Roehl, C. M., Wennberg, P. O., Warneke, T., and Landgraf, J.: Methane retrieved from TROPOMI: improvement of the data product and validation of the first 2 years of measurements, Atmos. Meas. Tech., 14, 665–684, https://doi.org/10.5194/amt-14-665-2021, 2021.

Lu, X., Jacob, D. J., Wang, H., Maasakkers, J. D., Zhang, Y., Scarpelli, T. R., Shen, L., Qu, Z., Sulprizio, M. P., Nesser, H., Bloom, A. A., Ma, S., Worden, J. R., Fan, S., Parker, R. J., Boesch, H., Gautam, R., Gordon, D., Moran, M. D., Reuland, F., Villasana, C. A. O., and Andrews, A.: Methane emissions in the United States, Canada, and Mexico: evaluation of national methane emission inventories and 2010–2017 sectoral trends by inverse analysis of in situ (GLOBALVIEWplus CH4 ObsPack) and satellite (GOSAT) atmospheric observations, Atmos. Chem. Phys., 22, 395–418, https://doi.org/10.5194/acp-22-395-2022, 2022.

Lunt, M. F., Palmer, P. I., Feng, L., Taylor, C. M., Boesch, H., and Parker, R. J.: An increase in methane emissions from tropical Africa between 2010 and 2016 inferred from satellite data, Atmos. Chem. Phys., 19, 14721–14740, https://doi.org/10.5194/acp-19-14721-2019, 2019.

Maasakkers, J., Omara, M., Gautam, R. et al., Reconstructing and quantifying methane emissions from the full duration of a 38-day natural gas well blowout using space-based observations. Remote Sensing of Environment. 270. 112755, doi:10.1016/j.rse.2021.112755, 2021.

Maasakkers JD, Varon DJ, Elfarsdóttir A, McKeever J, Jervis D, Mahapatra G, Pandey S, Lorente A, Borsdorff T, Foorthuis LR, Schuit BJ, Tol P, van Kempen TA, van Hees R, Aben I. Using satellites to uncover large methane emissions from landfills. Sci Adv., Aug 12;8(32). doi: 10.1126/sciadv.abn9683, 2022.

Ma, X., A. Huete, J. Cleverly, D. Eamus, F. Chevallier, J. Joiner, B. Poulter, Y. Zhang, L. Guanter, W. Meyer, Z. Xie, G. Ponce-Campos: Drought rapidly disseminates the 2011 large CO_2 uptake in semi-arid Australia. Scientific Reports, 6. doi: 10.1038/srep37747, 2016.

Mäder, J. A., J. Staehelin, D. Brunner, W. A. Stahel, I. Wohltmann, and T. Peter, Statistical modeling of total ozone: Selection of appropriate explanatory variables, *J. Geophys. Res.*, 112, D11108, doi:10.1029/2006JD007694, 2007.

Meirink, J. F., P. Bergamaschi, and M. Krol: Four-dimensional variational data assimilation for inverse modelling of atmospheric methane emissions: Method and comparison with synthesis inversion, *Atmos. Chem. Phys.*, 8, 6341–6353, 2008.

Monteil, G., Houweling, S., Butz, A., et al., Comparison of CH_4 inversions based on 15 months of GOSAT and SCIAMACHY observations, *J. Geophy. Res.*, doi: 10.1002/2013JD019760, Vol 118, Issue 20, 11807-11823, 2013.

Nassar, R., Hill, T. G., McLinden, C. A., Wunch, D., Jones, D. B. A., & Crisp, D., Quantifying CO_2 emissions from individual power plants from space. Geophysical Research Letters, 44, 10,045–10,053. https://doi.org/10.1002/2017GL074702, 2017.

O'Dell, C. W., Connor, B., Bösch, H., O'Brien, D., Frankenberg, C., Castano, R., Christi, M., Eldering, D., Fisher, B., Gunson, M., McDuffie, J., Miller, C. E., Natraj, V., Oyafuso, F., Polonsky, I., Smyth, M., Taylor, T., Toon, G. C., Wennberg, P. O., and Wunch, D.: The ACOS CO2 retrieval algorithm – Part 1: Description and validation against synthetic observations, *Atmos. Meas. Tech.*, 5, 99–121, doi:10.5194/amt-5-99-2012, 2012.

O'Dell, C. W., Eldering, A., Wennberg, P. O., Crisp, D., Gunson, M. R., Fisher, B., Frankenberg, C., Kiel, M., Lindqvist, H., Mandrake, L., Merrelli, A., Natraj, V., Nelson, R. R., Osterman, G. B., Payne, V. H., Taylor, T. E., Wunch, D., Drouin, B. J., Oyafuso, F., Chang, A., McDuffie, J., Smyth, M., Baker, D. F., Basu, S., Chevallier, F., Crowell, S. M. R., Feng, L., Palmer, P. I., Dubey, M., García, O. E., Griffith, D. W. T., Hase, F., Iraci, L. T., Kivi, R., Morino, I., Notholt, J., Ohyama, H., Petri, C., Roehl, C. M., Sha, M. K., Strong, K., Sussmann, R., Te, Y., Uchino, O., and Velazco, V. A.: Improved retrievals of carbon dioxide from Orbiting Carbon Observatory-2 with the version 8 ACOS algorithm, Atmos. Meas. Tech., 11, 6539–6576, https://doi.org/10.5194/amt-11-6539-2018, 2018.

Oda, T., and Maksyutov, S.: A very high-resolution (1 km×1 km) global fossil fuel CO2 emission inventory derived using a point source database and satellite observations of nighttime lights, *Atmos. Chem. Phys.*, 11, 543–556, doi:10.5194/acp-11-543-2011, 2011.

Olivier, J. G. J., van Aardenne, J. A., Dentener, F., Ganzeveld, L., and Peters, J. A. H. W.: Recent trends in global greenhouse gas emissions: regional trends and spatial distribution of key sources, in: Non-CO2 Greenhouse Gases (NCGG-4), edited by: van Amstel, A., Millpress, Rotterdam, 325–330, 2005.

Olivier, J. G. J., Janssens-Maenhout, G., and Peters, J. A. H. W., Trends in global CO_2 emissions, 2012 Report, PBL Netherlands Environmental Assessment Agency, The Hague, Joint Research Centre, Ispra, ISBN 978-92-79-25381-2, 2012.

Oshchepkov, S., A. Bril, T. Yokota, et al., Effects of atmospheric light scattering on spectroscopic observations of greenhouse gases from space. Part 2: Algorithm intercomparison in the GOSAT data processing for CO_2 retrievals over TCCON sites, *J. Geophys. Res.*, 118, 1493–1512, doi:10.1002/jgrd.50146, 2013.

	ESA Climate Change Initiative (CCI+)	Page 43
ghg cci	**Climate Assessment Report (CAR)** for Climate Research Data Package 8 (CRDP#8)	Version 1.0
	of the Essential Climate Variable (ECV) Greenhouse Gases (GHG)	8 February 2024

Osterman, G., and team (2022). Orbiting Carbon Observatory-2 & 3 (OCO-2 & OCO-3) – Data Product User's Guide, Operational Level 2 Lite Files – Version 2.0 – Revision A – July 5, 2022 – Data Release: 11 (OCO-2), 10/10.4 (OCO-3), https://docserver.gesdisc.eosdis.nasa.gov/public/project/OCO/OCO2_V11_OCO3_V10_DUG.pdf

Pandey, S., Houweling, S., Krol, M., Aben, I., Chevallier, F., Dlugokencky, E. J., Gatti, L. V., Gloor, M., Miller, J. B., Detmers, R., Machida, T., and Röckmann, T.: Inverse modeling of GOSAT-retrieved ratios of total column CH_4 and CO_2 for 2009 and 2010, *Atmos. Chem. Phys. Discuss.*, doi:10.5194/acp-2016-77, in review, 2016.

Parazoo, N. C., Bowman, K., Frankenberg, C., et al., Interpreting seasonal changes in the carbon balance of southern Amazonia using measurements of XCO_2 and chlorophyll fluorescence from GOSAT, *Geophys. Res. Lett.*, 40, 2829–2833, doi:10.1002/grl.50452, 2013.

Parker, R., Boesch, H., Cogan, A., et al., Methane Observations from the Greenhouse gases Observing SATellite: Comparison to ground-based TCCON data and Model Calculations, *Geophys. Res. Lett.*, doi:10.1029/2011GL047871, 2011.

Parker, R., Boesch, H., McNorton, J., et al. : Evaluating year-to-year anomalies in tropical wetland methane emissions using satellite CH_4 observations, Remote Sensing of Environment, 211, 261–275, doi:10.1016/j.rse.2018.02.011, 2018.

Peng, S., Lin, X., Thompson, R.L. et al. Wetland emission and atmospheric sink changes explain methane growth in 2020. Nature 612, 477–482, doi: 10.1038/s41586-022-05447-w, 2022.

Peters, W., Jacobson, A. R., Sweeney, C., et al.: An atmospheric perspective on North American carbon dioxide exchange: CarbonTracker, *Proceedings of the National Academy of Sciences* (*PNAS*) of the United States of America, 27 Nov. 2007, 104(48), 18925-18930, 2007.

Peylin, P., Law, R. M., Gurney, et al., Global atmospheric carbon budget: results from an ensemble of atmospheric CO_2 inversions, *Biogeosciences*, 10, 6699–6720, doi:10.5194/bg-10-6699-2013, URL http://www.biogeosciences.net/10/6699/2013/, 2013.

Pinty, B., G. Janssens-Maenhout, M. Dowell, H. Zunker, T. Brunhes, P. Ciais, D. Dee, H. Denier van der Gon, H. Dolman, M. Drinkwater, R. Engelen, M. Heimann, K. Holmlund, R. Husband, A. Kentarchos, Y. Meijer, P. Palmer and M. Scholze (2017) An operational anthropogenic CO_2 emissions monitoring & verification support capacity - Baseline requirements, Model components and functional architecture, doi:10.2760/39384, European Commission Joint Research Centre, EUR 28736 EN.

Poulter, B., Frank, D., Ciais, P., Myneni, R. B., Andela, N., Bi, J., Broquet, G. Canadell, J.G. Chevallier, F. Liu, Y. Y., Running, S. W., Sitch, S., and van der Werf, G. R.: Contribution of semi-arid ecosystems to interannual variability of the global carbon cycle. *Nature*, doi:10.1038/nature13376, 2014.

	ESA Climate Change Initiative (CCI+)	Page 44
ghg cci	**Climate Assessment Report (CAR)** for Climate Research Data Package 8 (CRDP#8)	Version 1.0
	of the Essential Climate Variable (ECV) Greenhouse Gases (GHG)	8 February 2024

Prather, M.: Interactive comment on "Carbon dioxide and climate impulse response functions for the computation of greenhouse gas metrics: a multi-model analysis" by F. Joos et al, Atmos. Chem. Phys. Discuss., 12, C8465–C8470, www.atmos-chem-phys-discuss.net/12/C8465/2012/, 2012.

Remaud, M., Chevallier, F., Cozic, A., Lin, X., and Bousquet, P.: On the impact of recent developments of the LMDz atmospheric general circulation model on the simulation of CO_2 transport, Geosci. Model Dev., 11, 4489–4513, https://doi.org/10.5194/gmd-11-4489-2018, 2018.

Reuter, M., Bovensmann, H., Buchwitz, M., et al., Retrieval of atmospheric CO_2 with enhanced accuracy and precision from SCIAMACHY: Validation with FTS measurements and comparison with model results, *J. Geophys. Res.*, 116, D04301, doi:10.1029/2010JD015047, 2011.

Reuter, M., Boesch, H., Bovensmann, H., et al., A joint effort to deliver satellite retrieved atmospheric CO_2 concentrations for surface flux inversions: the ensemble median algorithm EMMA, *Atmos. Chem. Phys.*, 13, 1771-1780, 2013.

Reuter, M., M. Buchwitz, M. Hilker, et al., Satellite-inferred European carbon sink larger than expected, *Atmos. Chem. Phys.*, 14, 13739-13753, doi:10.5194/acp-14-13739-2014, 2014a.

Reuter, M., M. Buchwitz, A. Hilboll, et al., Decreasing emissions of NOx relative to CO_2 in East Asia inferred from satellite observations, *Nature Geoscience*, 28 Sept. 2014, doi:10.1038/ngeo2257, pp.4, 2014b.

Reuter, M.: ESA Climate Change Initiative (CCI) Product User Guide version 4 (PUGv4) for the XCO2 SCIAMACHY Data Product BESD for the Essential Climate Variable (ECV): Greenhouse Gases (GHG), 31 August 2016, 2016a.

Reuter, M., M. Hilker, O. Schneising, M. Buchwitz, J. Heymann ESA Climate Change Initiative (CCI) Comprehensive Error Characterisation Report: BESD full-physics retrieval algorithm for XCO_2 for the Essential Climate Variable (ECV) Greenhouse Gases (GHG) Version 2.0, revision 1. 2016b.

Reuter, M., M. Buchwitz, M. Hilker, J. Heymann, H. Bovensmann, J. P. Burrows, S. Houweling, Y. Y. Liu, R. Nassar, F. Chevallier, et al., How much CO_2 is taken up by the European terrestrial biosphere?, Bulletin of the AmericanMeteorological Society, 0(0), doi:10.1175/BAMS-D-15-00310.1, 2016c.

Reuter, M., M. Buchwitz, O. Schneising, S. Noel, V. Rozanov, H. Bovensmann, J. P. Burrows, A Fast Atmospheric Trace Gas Retrieval for Hyperspectral Instruments Approximating Multiple Scattering - Part 1: Radiative Transfer and a Potential OCO-2 XCO_2 Retrieval Setup, Remote Sens., 9, 1159, doi:10.3390/rs9111159, 2017a.

Reuter, M., M. Buchwitz, O. Schneising, S. Noel, H. Bovensmann, J. P. Burrows, A Fast Atmospheric Trace Gas Retrieval for Hyperspectral Instruments Approximating Multiple Scattering - Part 2: Application to XCO_2 Retrievals from OCO-2, Remote Sens., 9, 1102, doi:10.3390/rs9111102, 2017b.

	ESA Climate Change Initiative (CCI+)	Page 45
ghg cci	**Climate Assessment Report (CAR)** for Climate Research Data Package 8 (CRDP#8)	Version 1.0
	of the Essential Climate Variable (ECV) Greenhouse Gases (GHG)	8 February 2024

Reuter, M., Buchwitz, M., Schneising, O., Krautwurst, S., O'Dell, C. W., Richter, A., Bovensmann, H., and Burrows, J. P.: Towards monitoring localized $CO2$ emissions from space: co-located regional CO_2 and NO_2 enhancements observed by the OCO-2 and S5P satellites, Atmos. Chem. Phys., 19, 9371–9383, https://doi.org/10.5194/acp-19-9371-2019, 2019.

Reuter, M., Buchwitz, M., Schneising, O., Noël, S., Bovensmann, H., Burrows, J. P., Boesch, H., Di Noia, A., Anand, J., Parker, R. J., Somkuti, P., Wu, L., Hasekamp, O. P., Aben, I., Kuze, A., Suto, H., Shiomi, K., Yoshida, Y., Morino, I., Crisp, D., O'Dell, C. W., Notholt, J., Petri, C., Warneke, T., Velazco, V. A., Deutscher, N. M., Griffith, D. W. T., Kivi, R., Pollard, D. F., Hase, F., Sussmann, R., Té, Y. V., Strong, K., Roche, S., Sha, M. K., De Mazière, M., Feist, D. G., Iraci, L. T., Roehl, C. M., Retscher, C., and Schepers, D.: Ensemble-based satellite-derived carbon dioxide and methane column-averaged dry-air mole fraction data sets (2003–2018) for carbon and climate applications, Atmos. Meas. Tech., 13, 789–819, https://doi.org/10.5194/amt-13-789-2020, 2020.

Rödenbeck, C.: Estimating CO_2 sources and sinks from atmospheric mixing ratio measurements using a global inversion of atmospheric transport, Tech. Rep. 6, Max Planck Institute for Biogeochemistry, Jena, Germany, 2005.

Ross, A. N., Wooster, M. J., Boesch, H., Parker, R., First satellite measurements of carbon dioxide and methane emission ratios in wildfire plumes, *Geophys. Res. Lett.*, 40, 1-5, doi:10.1002/grl.50733, 2013.

Scarcle, J. D., Studies in astronomical time series analysis. III. Fourier transforms, autocorrelation functions and cross-correlation functions of unevenly spaced data. *Astrophys. J.*, 343, 874–887, 1989.

Schneising, O., Buchwitz, M., Reuter, M., et al., Long-term analysis of carbon dioxide and methane column-averaged mole fractions retrieved from SCIAMACHY, *Atmos. Chem. Phys.*, 11, 2881-2892, 2011.

Schneising, O., J. Heymann, M. Buchwitz, M. Reuter, H. Bovensmann, and J. P. Burrows, Anthropogenic carbon dioxide source areas observed from space: assessment of regional enhancements and trends, *Atmos. Chem. Phys.*, 13, 2445-2454, 2013.

Schneising, O., M. Reuter, M. Buchwitz, J. Heymann, H. Bovensmann, and J. P. Burrows, Terrestrial carbon sink observed from space: variation of growth rates and seasonal cycle amplitudes in response to interannual surface temperature variability, *Atmos. Chem. Phys.*, 14, 133-141, 2014a.

Schneising, O., J. P. Burrows, R. R. Dickerson, M. Buchwitz, M. Reuter, H. Bovensmann, Remote sensing of fugitive methane emissions from oil and gas production in North American tight geologic formations, *Earth's Future*, 2, DOI: 10.1002/2014EF000265, pp. 11, 2014b.

Schneising, O., Buchwitz, M., Reuter, M., Bovensmann, H., Burrows, J. P., Borsdorff, T., Deutscher, N. M., Feist, D. G., Griffith, D. W. T., Hase, F., Hermans, C., Iraci, L. T., Kivi, R., Landgraf, J., Morino, I., Notholt, J., Petri, C., Pollard, D. F., Roche, S., Shiomi, K., Strong, K., Sussmann, R., Velazco, V. A.,

	ESA Climate Change Initiative (CCI+)	Page 46
ghg cci	**Climate Assessment Report (CAR)** for Climate Research Data Package 8 (CRDP#8)	Version 1.0
	of the Essential Climate Variable (ECV) Greenhouse Gases (GHG)	8 February 2024

Warneke, T., and Wunch, D.: A scientific algorithm to simultaneously retrieve carbon monoxide and methane from TROPOMI onboard Sentinel-5 Precursor, Atmos. Meas. Tech., 12, 6771–6802, https://doi.org/10.5194/amt-12-6771-2019, 2019.

Schneising, O., Buchwitz, M., Reuter, M., Vanselow, S., Bovensmann, H., and Burrows, J. P.: Remote sensing of methane leakage from natural gas and petroleum systems revisited, Atmos. Chem. Phys., 20, 9169–9182, https://doi.org/10.5194/acp-20-9169-2020, 2020.

Schulze, E. D., Luyssaert, S., Ciais, P., Freibauer, A., Janssens, I. A., Soussana, J. F., Smith, P., Grace, J., Levin, I., Tiruchittampalam, B., Heimann, M., Dolman, A. J., Valentini, R., Bousquet, P., Peylin, P., Peters, W., Rodenbeck, C., Etiope, G., Vuichard, N., Wattenbach, M., Nabuurs, G. J., Poussi, Z., Nieschulze, J., Gash, J. H., and Team, C.: Importance of methane and nitrous oxide emissions for europe's terrestrial greenhouse gas balance, *Nat. Geosci*., 2, 842–850, 2009.

Shen, L., Jacob, D.J., Gautam, R. et al. National quantifications of methane emissions from fuel exploitation using high resolution inversions of satellite observations. Nat Commun 14, 4948, doi:10.1038/s41467-023-40671-6, 2023.

Shindell, D. T., O. Pechony, A. Voulgarakis, et al., Interactive ozone and methane chemistry in GISS-E2 historical and future climate simulations, *Atmos. Chem. Phys.*, 13, 2653–2689, doi:10.5194/acp-13-2653-2013, 2013.

Somkuti, P.: ESA Climate Change Initiative (CCI) Product User Guide version 4.0 (PUGv4.0) for the University of Leicester full-physics XCO_2 GOSAT data product (CO2_GOS_OCFP version 7) for the Essential Climate Variable (ECV): Greenhouse Gases (GHG), 31 August 2016, 2016.

Sussmann, R., Forster, F., Rettinger, M., and Bousquet, P.: Renewed methane increase for five years (2007–2011) observed by solar FTIR spectrometry, Atmos. Chem. Phys., 12, 4885-4891, doi:10.5194/acp-12-4885-2012, 2012.

Turner, A. J., Jacob, D. J., Wecht, K. J., Maasakkers, J. D., Lundgren, E., Andrews, A. E., Biraud, S. C., Boesch, H., Bowman, K. W., Deutscher, N. M., Dubey, M. K., Griffith, D. W. T., Hase, F., Kuze, A., Notholt, J., Ohyama, H., Parker, R., Payne, V. H., Sussmann, R., Sweeney, C., Velazco, V. A., Warneke, T., Wennberg, P. O., and Wunch, D.: Estimating global and North American methane emissions with high spatial resolution using GOSAT satellite data, *Atmos. Chem. Phys*., 15, 7049-7069, doi:10.5194/acp-15-7049-2015, 2015.

Varon, D. J., Jacob, D. J., Hmiel, B., Gautam, R., Lyon, D. R., Omara, M., Sulprizio, M., Shen, L., Pendergrass, D., Nesser, H., Qu, Z., Barkley, Z. R., Miles, N. L., Richardson, S. J., Davis, K. J., Pandey, S., Lu, X., Lorente, A., Borsdorff, T., Maasakkers, J. D., and Aben, I.: Continuous weekly monitoring of methane emissions from the Permian Basin by inversion of TROPOMI satellite observations, Atmos. Chem. Phys., 23, 7503–7520, https://doi.org/10.5194/acp-23-7503-2023, 2023.

Wanninkhof, R., Park, G. -H., Takahashi, T., Sweeney, C., Feely, R., Nojiri, Y., Gruber, N., Doney, S. C., McKinley, G. A., Lenton, A., Le Quéré, C., Heinze, C., Schwinger, J., Graven, H., and Khatiwala, S.: Global ocean carbon uptake: magnitude, variability and trends, *Biogeosciences*, 10, 1983-2000, doi:10.5194/bg-10-1983-2013, 2013.

van der Werf, G. R., Randerson, J. T., Giglio, L., Collatz, G. J., Mu, M., Kasibhatla, P. S., Morton, D. C., DeFries, R. S., Jin, Y., and van Leeuwen, T. T.: Global fire emissions and the contribution of deforestation, savanna, forest, agricultural, and peat fires (1997–2009), *Atmos. Chem. Phys.*, 10, 11707-11735, doi:10.5194/acp-10-11707-2010, 2010.

Wecht, K. J., D. J. Jacob, C. Frankenberg, Z. Jiang, and D. R. Blake (2014), Mapping of North American methane emissions with high spatial resolution by inversion of SCIAMACHY satellite data, J. Geophys. Res. Atmos., 119, 7741–7756, doi:10.1002/2014JD021551.

Wunch, D., Toon, G. C., Blavier, J.-F., et al., The Total Carbon Column Observing Network, *Phil. Trans. R. Soc. A*, 369, 2087–2112, doi:10.1098/rsta.2010.0240, 2011.

Wunch, D., Wennberg, P. O., Toon, G. C. et al., A method for evaluating bias in global measurements of CO_2 total columns from space. Atmos. Chem. Phys., 11, 12317-12337, 2011.

Yang, D. X., and Coauthors, 2021: A new TanSat XCO2 global product towards climate studies. Adv. Atmos. Sci., 38(1), 8–11, https://doi.org/10.1007/s00376-020-0297-y.

Yin, Y., Chevallier, F., Ciais, P., Bousquet, P., Saunois, M., Zheng, B., Worden, J., Bloom, A. A., Parker, R. J., Jacob, D. J., Dlugokencky, E. J., and Frankenberg, C.: Accelerating methane growth rate from 2010 to 2017: leading contributions from the tropics and East Asia, Atmos. Chem. Phys., 21, 12631–12647, https://doi.org/10.5194/acp-21-12631-2021, 2021.

Yoshida, Y., Kikuchi, N., Morino, I., et al., Improvement of the retrieval algorithm for GOSAT SWIR XCO_2 and XCH_4 and their validation using TCCON data, *Atmos. Meas. Tech.*, 6, 1533–1547, doi:10.5194/amt-6-1533-2013, 2013.

Zhang, Y., Gautam, R., Pandey, S. et al., Quantifying methane emissions from the largest oil-producing basin in the United States from space. Sci. Adv. 6, 17, doi:10.1126/sciadv.aaz5120, 2020.

END OF DOCUMENT